
Predictive Complexity Priors

Eric Nalisnick, Jonathan Gordon, José Miguel Hernández-Lobato

Department of Engineering
University of Cambridge
{etn22, jg801, jmh233}@cam.ac.uk

Abstract

Specifying a Bayesian prior is notoriously difficult for complex models such as neural networks. Reasoning about parameters is made challenging by the high-dimensionality and over-parameterization of the space. Priors that seem benign and uninformative can have unintuitive and detrimental effects on a model’s predictions. For this reason, we propose *predictive complexity priors*: a functional prior that is defined by comparing the model’s predictions to those of a reference function. Although originally defined on the model outputs, we transfer the prior to the model parameters via a change of variables. The traditional Bayesian workflow can then proceed as usual. We apply our predictive complexity prior to modern machine learning tasks such as reasoning over neural network depth and sharing of statistical strength for few-shot learning.

1 Introduction

Choosing the prior for a Bayesian model is the most important—and often, the most difficult—step in model specification [45]. Unfortunately, prior specification within machine learning is additionally fraught and challenging. Popular models such as neural networks (NNs) are high dimensional and unidentifiable, making it extremely hard to reason about what makes a good prior. Moreover, since the true posterior can almost never be recovered, it is difficult to isolate a prior’s influence (even empirically). We are left asking: do the specifics of the prior even matter if they are blunted by our posterior approximations and large data sets? Until recently, most work in machine learning has assumed the negative and resorted to priors of convenience. For instance, the standard normal distribution is by far the most popular prior for Bayesian NNs [58, 24, 55].

Lately, there is mounting evidence that the choice of prior for Bayesian NNs does indeed have a significant influence. For instance, Wenzel et al. [55] show that the standard normal prior leads to poor models and requires tempering to mitigate the misspecification. In light of these issues, recent work has proposed priors that can be defined in function space [15, 50, 36, 3, 33, 22, 16, 42, 32]. The hope is that it is easier to reason about our preferences for functions than for parameters. However, existing functional priors introduce cumbersome byproducts into the Bayesian workflow. Placing a functional prior on a NN requires either taking infinite width limits [42], optimizing divergences involving stochastic processes [15, 50], or pre-training [15, 36, 3].

In this paper, we contribute to this line of work by specifying a Bayesian prior on the model’s *functional complexity*. Our prior, termed the *predictive complexity prior* (PredCP), compares the model’s predictions to those of a reference function. For example, we define the reference model for a NN to be a NN with one fewer layer. The PredCP can then assess and control the effect of depth on the model’s capacity. Unlike previous work on functional priors, we use a change of variables to *exactly* translate the functional prior into a proper prior on the model parameters. Bayesian inference can then proceed as usual and without involving extra machinery. We claim the following contributions:

- **Methodology:** We propose *Predictive Complexity Priors* (PredCPs). These extend Simpson et al. [47]’s framework to the model predictions, thereby allowing our data-space intuitions to guide prior specification. Moreover, we introduce crucial modifications that allow the PredCP to scale to large, black-box models such as NNs.
- **Applications:** We demonstrate the wide applicability of the PredCP by using it for two disparate tasks: reasoning over depth in Bayesian NNs and sharing information across tasks for few-shot learning. For the former, we investigate the PredCP’s behavior in detail, revealing its mechanism of action: regularizing predictive variance.
- **Experiments:** We report results across a variety of tasks (classification, regression, few-shot learning), models (logistic regression, NNs), and posterior inference strategies (Markov chain Monte Carlo, variational inference, MAP estimation). The PredCP provides consistent improvements in predictive generalization over alternative priors (uninformative, shrinkage).

2 Background: Penalized Complexity Priors

Notation Matrices are denoted with upper-case and bold letters (e.g. \mathbf{Y}), vectors with lower-case and bold (e.g. \mathbf{y}), and scalars with no bolding (e.g. y or Y). We use italics to differentiate observations and constants (e.g. \mathbf{y} , θ) from random variables (e.g. \mathbf{y} , θ).

Given the difficulty in choosing a prior, Simpson et al. [47] had the insight of incorporating the selection process into prior specification itself. Let $p_0(\theta)$ denote a ‘base’ prior and $p_+(\theta)$ an ‘extended’ prior. The base prior is assumed to be less expressive than the extended one, possibly via a restricted support. A common conundrum is choosing between $p_0(\theta)$ and $p_+(\theta)$. The former may guard against overfitting but at the risk of its regularization hampering the model’s fit. Conversely, the latter’s flexibility may result in a spurious solution. Simpson et al. [47] propose a hyperprior that smoothly interpolates between the two and captures their functional difference.

They begin by defining the Kullback–Leibler divergence (KLD) between the two priors: $\text{KL}[p_+(\theta|\tau) || p_0(\theta)]$ where τ is a hyper-parameter that controls p_+ ’s complexity. The asymmetry of the KLD is desired in this setting since $\text{KL}[p_+ || p_0]$ represents the information lost when using p_0 to approximate p_+ . Switching the directionality would not be sensible since p_+ can easily approximate p_0 . Simpson et al. [47] then derive a prior for τ by placing a distribution on the root-KLD and performing a change of variables:

$$\pi(\tau; \lambda) = \pi_{\text{KL}}\left(\sqrt{2\text{KL}[p_+(\theta|\tau) || p_0(\theta)]}; \lambda\right) \left| \frac{\partial \sqrt{2\text{KL}[p_+(\theta|\tau) || p_0(\theta)]}}{\partial \tau} \right| \quad (1)$$

where $\pi_{\text{KL}}(\cdot; \lambda)$ is the prior on the root-KLD with parameters λ and $|\partial\sqrt{2\text{KL}}/\partial\tau|$ denotes the absolute value of the root-KLD’s derivative w.r.t. τ . This second term on the RHS arises from the change of variables and ensures the resulting prior on τ is proper (integrates to one). For the change of variables to be well-defined, the KLD must be bijective and differentiable w.r.t. τ . The square root removes the KLD’s intrinsic power of two, and the factor of two is introduced for convenience.

Simpson et al. [47] term $\pi(\tau)$ a *penalized complexity prior* (PCP) since it encodes how deviation from the base prior (via τ) should be penalized. For a simple example of a PCP, consider the priors: $p_0 = \lim_{\sigma \rightarrow 0^+} \text{N}(0, \sigma)$ and $p_+ = \text{N}(0, \tau)$. Using an exponential distribution for π_{KL} , Simpson et al. [47] show the resulting PCP on τ is a type-II Gumbel distribution. PCPs have since been used as priors for P-splines [51], distributional regression [30], autoregressive processes [49], mixed effects models [52], and Gaussian random fields [17].

3 Idealized Setting: Evidence Complexity Priors

We now consider how a PCP-like prior could be formulated for complex models such as NNs. The PCP, as is, is not well-suited because it still requires intimate knowledge of parameter space. Specifying the base prior, which grounds the model of interest, runs into the same challenges of high-dimensionality and unidentifiability. Rather, we need a prior that is derived by taking a holistic perspective of the model [20] and with a clear connection to the space in which data resides.

In this section, we describe a variant of the PCP that meets these criterion. We call it the *evidence complexity prior* (ECP) as it is defined via the model evidence. Unfortunately, the ECP is still

not widely applicable to complex models because it requires an integration step that is usually intractable. Yet, we present the ECP first—before moving on to a more scalable and widely applicable alternative—to make clear the ideas that underpin both priors. In other words, the ECP is derived in an idealized setting and used as a conceptual stepping stone between the PCP and our *predictive complexity prior* (introduced in the next section). The ECP is derived via the following three steps.

Step #1: Define Base and Extended Models Following Simpson et al. [47], we consider base and extended priors. Yet here we work with their marginalized forms:

$$p_0(\mathbf{y}) = \int_{\boldsymbol{\theta}} p(\mathbf{y}|\boldsymbol{\theta}) p_0(\boldsymbol{\theta}) d\boldsymbol{\theta}, \quad p_+(\mathbf{y}|\tau) = \int_{\boldsymbol{\theta}} p(\mathbf{y}|\boldsymbol{\theta}) p_+(\boldsymbol{\theta}|\tau) d\boldsymbol{\theta} \quad (2)$$

where $p(\mathbf{y}|\boldsymbol{\theta})$ denotes the data model. The priors $p_0(\boldsymbol{\theta})$ and $p_+(\boldsymbol{\theta}|\tau)$ are defined just as above for PCPs. Again τ is a scalar that controls the complexity of p_+ and is ultimately our variable of interest. Crucially, \mathbf{y} denotes a *random variable* that corresponds to data, not an observation (which would be denoted \mathbf{y}). Thus, we call $p_0(\mathbf{y})$ and $p_+(\mathbf{y}|\tau)$ ‘evidence functions’ [5] to make clear that they are independent of data. For many models, it will be hard to perform the above integration, which is why we referred to the ECP’s construction as ‘idealized.’

Step #2: KLD Prior We next place a prior $\pi_{\text{KL}}(\cdot; \boldsymbol{\lambda})$ on the KLD between these marginal distributions: $\pi_{\text{KL}}(\text{KL}[p_+(\mathbf{y}|\tau) || p_0(\mathbf{y})]; \boldsymbol{\lambda})$ where $\boldsymbol{\lambda}$ are the parameters of π_{KL} . We assume $p_0(\mathbf{y})$ and $p_+(\mathbf{y}|\tau)$ both have full support over $\mathbf{y} \in \mathcal{Y}$, which should ensure the divergence is finite in most cases. The support of π_{KL} should be $\mathbb{R}^{\geq 0}$ to match the KLD’s codomain. If π_{KL} ’s support is \mathbb{R}^+ , then we assume a small constant is added to the KLD so that it never evaluates to exactly zero. We drop the factor of two and square root that are in the PCP’s formulation.

Step #3: Change Variables Again following the PCP, we perform a change of variables to define a prior on τ . The ECP’s final form is then:

$$\pi(\tau; \boldsymbol{\lambda}) = \pi_{\text{KL}}(\text{KL}[p_+(\mathbf{y}|\tau) || p_0(\mathbf{y})]; \boldsymbol{\lambda}) \left| \frac{\partial \text{KL}[p_+(\mathbf{y}|\tau) || p_0(\mathbf{y})]}{\partial \tau} \right|. \quad (3)$$

The ECP is proper when the KLD is bijective and differentiable w.r.t. τ . We will discuss these conditions for NNs in Section 5. Despite its dependence on the observation model, the ECP is not an empirical Bayesian prior [10] since \mathbf{y} is integrated out when computing the KLD.

The crucial characteristics of the ECP are that it compares the models holistically and in data space. Using the evidence functions (step #1) allows the ECP to directly assess how τ affects \mathbf{y} . Hence the ECP embraces the philosophy that the prior can only be understood in the context of the likelihood [20]. Computing the KLD (step #2) then provides a functional comparison of how the models allocate probability in data space. This data-space behavior is our ultimate concern for black-box models.

3.1 Example: Linear Regression

We continue discussion of the ECP with a concrete example. Consider the linear model $\mathbb{E}[y|x, \beta] = x\beta$, where $y \in \mathbb{R}$ denotes a scalar response, $x \in \mathbb{R}$ its covariate / feature, and $\beta \in \mathbb{R}$ the model parameter. While this is undoubtedly a simple example, the priors we later describe for NNs will have commonalities. Let us now step through the ECP derivation. We choose the extended prior to be normal, $p_+(\beta|\tau) = \text{N}(0, \tau)$, and the base prior to be ‘the spike,’ $p_0(\beta) = \delta(|\beta - 0|)$. The ECP for τ is then:

$$\begin{aligned} \pi(\tau; \lambda, x) &= \pi_{\text{KL}}(\text{KL}[\text{N}(0, \sigma_y^2 + x^2\tau) || \text{N}(0, \sigma_y^2)]; \lambda) \left| \frac{\partial \text{KL}[\text{N}(0, \sigma_y^2 + x^2\tau) || \text{N}(0, \sigma_y^2)]}{\partial \tau} \right| \\ &= \pi_{\text{KL}}\left(\frac{-1}{2} \log(1 + \sigma_y^{-2} x^2 \tau) + \frac{x^2 \tau}{2\sigma_y^2}; \lambda\right) \left| \frac{x^2}{2\sigma_y^2} - \frac{x^2}{2(\sigma_y^2 + x^2\tau)} \right|. \end{aligned} \quad (4)$$

where σ_y^2 is the response noise. In this case—and for conditional models in general—the ECP is a function of the features x and any other independent variables. Other default priors such as the *g-prior* [57] and Jeffreys prior [26] have this dependence as well, which reflects their holistic natures.

Choosing π_{KL} We next discuss the choice of π_{KL} and its effect on the resulting ECP. Figure 1(b) shows three ECPs, each defined by a different choice of KLD prior (1(a)): exponential (green),

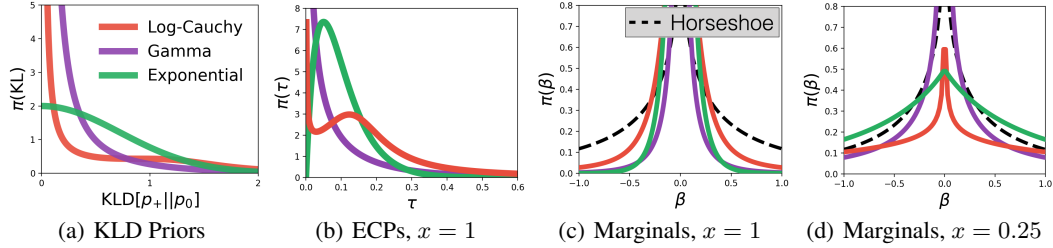


Figure 1: *ECP for Linear Regression*. Subfigure (a) shows each KLD prior: exponential ($\lambda = .5$), gamma ($\lambda = (.2, 2)$), and log-Cauchy ($\lambda = 1$). Subfigure (b) shows the corresponding ECP on τ . Subfigure (c) shows the marginal prior on β induced by each ECP from (b). Subfigure (c) shows the same marginals for $x = 0.25$. The horseshoe prior [9] (black dashed line) is shown for reference. The ECP adapts with the input feature, resulting in dynamic shrinkage properties.

gamma (purple), and log-Cauchy (red). The choice of π_{KL} is significant. First considering the exponential prior, it clearly favors $\tau > 0$ since the density function decays to zero at the origin. We can interpret this behavior in the context of the base and extended models as a strict preference for p_+ . At the other extreme is the gamma prior: it has a mode at $\tau = 0$ and then quickly decays as τ increases. Thus, the gamma strictly prefers p_0 . Last we have the log-Cauchy, which we chose due to its heavy tail. Heavy-tailed priors have been well-validated for robust regression since they allow the shrinkage to be ignored under sufficient counter-evidence [9]. A similar logic can be applied to the KLD: perhaps the base model is too simplistic and p_+ is drastically superior. If so, we want any preference for the base model to be forgotten. Figure 1(b) shows that the log-Cauchy results in an ECP with two modes, one at $\tau = 0$ and another at $\tau \approx .15$. The log-Cauchy is able to balance its preferences for p_+ and p_0 , interpolating between the exponential and gamma’s single-mindedness.

Marginal Priors and Feature Dependence It is perhaps more intuitive to examine the marginal prior on β induced by the ECP: $\pi(\beta) = \int p(\beta|\tau)\pi(\tau)d\tau$. Figure 1(c) shows the marginal prior for the three ECPs considered above and compares them to the horseshoe prior [9] (black dashed line). The three priors behave as expected from looking at $\pi(\tau)$: the gamma shrinks the hardest and the log-Cauchy has the heaviest tails. Yet, recall that the ECP also depends on x . So far we have assumed $x = 1$, but in Figure 1(d) we show the same marginal priors for $x = 0.25$. This change in x results in drastically different ECPs. As $x \rightarrow 0$, the ECP (no matter the choice of π_{KL}) becomes heavier tailed, allowing more deviation from the base model. This behavior is natural since, when x is small, large β values are necessary to substantially change the model’s predictions. See Appendix A for more discussion, including of shrinkage profiles and the ECP for multivariate regression.

4 Extension to Black-Box Models: Predictive Complexity Priors

We now move on to our primary contribution: deriving a prior that has the same holistic, function-space properties as the ECP but is tractable for models such as NNs. As mentioned earlier, the primary weakness of the ECP is the difficulty of step #1: integrating over θ . In this section, we propose modifications to the ECP derivation that result in a tractable and scalable alternative. We call the resulting prior a *predictive complexity prior* (PredCP).

Point-Mass Base Priors We first address integrating over the base prior in step #1. From here forward, we assume that the base model is defined by a point-mass (Dirac delta) prior. In turn, the marginalization in step #1 becomes trivial:

$$p_0(\mathbf{y}) = \int_{\theta} p(\mathbf{y}|\theta) \delta(|\theta - \theta_0|) d\theta = p(\mathbf{y}|\theta_0). \quad (5)$$

A benefit of comparing the models in \mathcal{Y} -space is that the base prior can have strictly smaller support than the extended, as is the case when using point-mass priors. The PCP, on the other hand, can not easily support point-mass priors and must instead be defined by taking limits [47].

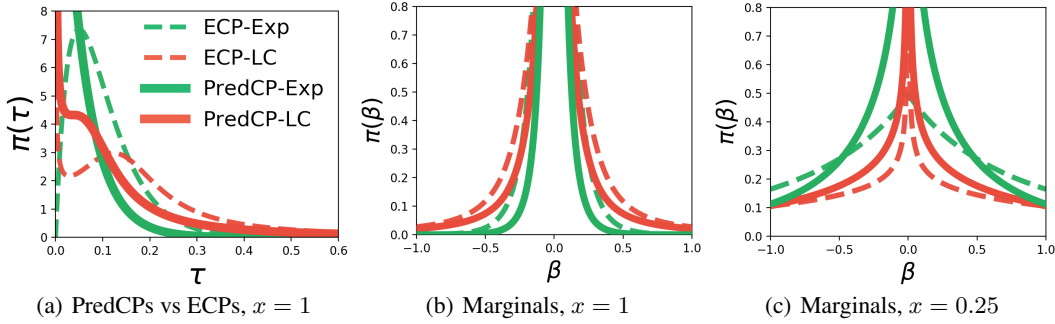


Figure 2: *PredCP for Linear Regression*. Subfigure (a) compares the ECP (dashed lines) vs the PredCP (solid lines) for the exponential and log-Cauchy KLD priors ($x = 1$). Subfigures (b) and (c) compare the marginal priors at $x = 1$ and $x = .25$ respectively.

KLD Upper Bound The next obstacle is integrating over the extended model’s prior. We make headway by defining the PredCP using the following upper bound on the ECP’s KLD:

$$\text{KL} [p_+(y|\tau) \parallel p_0(y)] = \text{KL} [\mathbb{E}_{\theta|\tau} [p_+(y|\theta)] \parallel p(y|\theta_0)] \leq \mathbb{E}_{\theta|\tau} \text{KL} [p(y|\theta) \parallel p(y|\theta_0)]. \quad (6)$$

We arrive at the upper bound via Jensen’s inequality. The bound essentially reverses the order in which marginalization and divergence computation are done for the ECP. This reversal makes the PredCP more practical since its KLD is taken between the data models. These are usually simple distributions (e.g. categorical, Gaussian) that afford a closed-form KLD. Unfortunately, the expectation over $\theta|\tau$ may still not be analytically available. We recommend evaluating the integral using a *differentiable, non-centered* Monte Carlo (MC) approximation [29]. Doing so ensures the KLD’s derivative w.r.t. τ is well-defined. For supervised learning, a downside of the upper bound is that the dependencies between predictions are lost. Having the data model factorize across observations— $p(\mathbf{Y}|\mathbf{X}, \theta) = \prod_n p(y|x_n, \theta)$ —results in the KLD becoming a point-wise sum.

Mini-Batching For supervised learning, evaluating the PredCP requires a sum over all feature observations, which will be computationally costly for large data sets. Therefore we recommend the PredCP be evaluated with mini-batches. Moreover, we compute the KLD’s mean across the mini-batch, not the sum. In doing so we assume that the batch’s mean KLD represents an unbiased estimate of the full-data mean KLD. We use the mean KLD primarily for practical purposes: it is easier to set the prior’s parameters λ since they do not have to account for the batch size.

PredCP Final Form Below we give the final form of the PredCP for supervised learning, combining the point-mass base prior, the KLD upper bound, and mini-batching:

$$\pi(\tau; \lambda, \mathbf{X}_B) = \pi_{\text{KL}} \left(\frac{1}{B} \sum_{b=1}^B \mathbb{E}_{\theta|\tau} \text{KL} [p(y|x_b, \theta) \parallel p(y|x_b, \theta_0)]; \lambda \right) \left| \frac{1}{B} \sum_{b=1}^B \frac{\partial \mathbb{E}_{\theta|\tau} \text{KL}_b}{\partial \tau} \right| \quad (7)$$

where b indexes the B -sized batch and $\mathbb{E}_{\theta|\tau} \text{KL}_b$ is shorthand for the expected KLD for the b th instance. The PredCP encourages stronger shrinkage than the ECP, which is expected due to the upper bound. For a given τ , the PredCP deems the models to be more discrepant than the ECP would for the same τ . This is an appropriate inductive bias for the PredCP since it will be used for large models that often require strong regularization. In Figure 2, we compare the ECP (dashed lines) and the corresponding PredCP (solid lines) for the linear regression example. The PredCP’s inductive bias (from the upper bound) is evident in the leftward shift of the density functions. This shift can change the PredCP’s behavior considerably in comparison to the corresponding ECP. The exponential’s PredCP has a mode at $\tau = 0$ whereas its ECP decays to zero at the origin.

5 Applications of the PredCP

We now demonstrate the PredCP’s utility for modern machine learning. We consider two applications: depth-selection for Bayesian NNs [12, 37, 2] and sharing statistical strength across tasks for meta-

learning [11]. Both of these applications exhibit the PredCP’s ability to enable Bayesian reasoning across the model’s macro-structures (e.g. layers) while still being a tractable and proper prior.

Bijection Conditions for Neural Networks Before moving on to these two applications, we first address some technical conditions. Recall that for the PredCP to be a proper prior (i.e. integrate to one), the expected KLD must be differentiable and bijective w.r.t. τ . The former is easy to satisfy by using a non-centered MC approximation, as mentioned above. It is not obvious if the latter is satisfied by NNs. One could check the condition via brute force, by using numerical integration. Since τ is a scalar, the numerical solution should be stable and makes for a good unit test. Yet, we show in Appendix B that bijectivity is satisfied for feedforward NNs with ReLU activations and Gaussian or categorical observation models. No architectural modifications are necessary.

Depth Selection for Bayesian Neural Networks PredCPs allow us to perform Bayesian reasoning over the depth of a NN. First assume the NN to be a residual network (resnet) [23]; later we will address the traditional feedforward case. Since we wish to isolate the effect of depth, we choose the base model to be a NN with $l - 1$ layers and the extended model to be the same NN but with an additional layer (l total layers). The KLD between these models will then capture the extra capacity afforded by the additional layer. More formally, for an arbitrary layer l , the prior on the (square) weight matrix $\mathbf{W}_l \in \mathbb{R}^{D_h \times D_h}$ for the base and extended models are: $p_0(\mathbf{W}_l) = \delta(|\mathbf{W}_l - \mathbf{0}|)$, $p_+(\mathbf{W}_l|\tau_l) = \mathbf{N}(\mathbf{0}, \tau_l \Sigma_l)$ where τ_l is again the parameter of interest controlling the capacity of the extended model. Integrating over p_0 sets $\mathbf{W}_k = \mathbf{0}$ for $k \geq l$ for the base model and $k > l$ for the extended model. The resnet then maps the hidden layers directly to the output layer, thereby allowing the PredCP to compare the predictions when using $l - 1$ vs l layers. We can define the PredCP for all layers by applying the above priors recursively from the bottom-up:

$$\begin{aligned} \pi(\tau_1, \dots, \tau_L) &= \pi(\tau_1) \prod_{l=2}^L \pi(\tau_l | \tau_1, \dots, \tau_{l-1}) \\ &= \prod_{l=1}^L \pi_{\text{KL}} \left(\mathbb{E}_{\{\mathbf{w}_j | \tau_j\}_{j=1}^l} \text{KL} [p_+(y | \mathbf{X}, \{\mathbf{W}_j\}_{j=1}^l) || p_0(y | \mathbf{X}, \{\mathbf{W}_k\}_{k=1}^{l-1})] \right) \left| \frac{\partial \mathbb{E} \text{KL}_l}{\partial \tau_l} \right| \end{aligned} \quad (8)$$

where $\mathbb{E} \text{KL}$ serves as shorthand for the expected KLD inside π_{KL} . Computing the full prior requires L forward propagations, each evaluating a progressively deeper network with the hidden units at layer l serving as the last hidden layer. In practice, we cache the forward propagation required to evaluate the extended model for τ_l and use it as the base model when evaluating the prior for τ_{l+1} . Nearly the same procedure can be applied to non-residual networks, except that the residual connections can no longer be relied upon to transport the hidden units to the output layer. Rather, the network must be ‘short circuited,’ with the final hidden units being directly multiplied with the output weights. Figure 3(a) shows the joint density function $\pi(\tau_1, \tau_2)$ for both traditional and residual NNs. The PredCP’s capability for depth selection is conspicuous for the traditional NN (left). The high density region (red) touches the x -axis but not the y -axis except near the origin. This implies that τ_2 cannot grow unless $\tau_1 > 0$, meaning that the first layer is activated. For resnets (right), the density’s L -shape means that either layer can be active while the other is inactive ($\tau \approx 0$), which is made possible by the skip connection. Yet the density’s bias towards the x -axis suggests that the resnet-PredCP still prefers to activate τ_1 ’s layer before activating τ_2 ’s.

Further intuition can be had by examining the depth-wise PredCP for resnets with a Gaussian data model. Denote a hidden layer for the n th observation as $\mathbf{h}_{n,l} = \mathbf{h}_{n,l-1} + f_l(\mathbf{h}_{n,l-1} \mathbf{W}_l)$ and the output weights as $\mathbf{W}_o \sim \mathbf{N}(\mathbf{0}, \Sigma)$. We assume \mathbf{W}_l is parameterized as $\sqrt{\tau_l} \tilde{\mathbf{W}}_l$, $\tilde{\mathbf{W}}_l \sim \mathbf{N}(\mathbf{0}, \Sigma)$. The expected KLD for computing $\pi(\tau_l | \tau_{1:l-1})$ (Equation 8) is then:

$$\mathbb{E}_{\{\mathbf{w}_j | \tau_j\}_{j=1}^l} \text{KL} [p_+ || p_0] = \frac{\tau_l}{2\sigma_y^2} \frac{1}{N} \sum_{n=1}^N \text{Var}_{\tilde{\mathbf{w}}, \mathbf{w}_o} [f_l(\mathbf{h}_{n,l-1} \tilde{\mathbf{W}}_l) \mathbf{W}_o] \quad (9)$$

where σ_y^2 denotes the response noise and f_l is any positively homogeneous activation function (such as the ReLU). The crucial term $\text{Var}[f_l \mathbf{W}_o]$ represents the variance that the l th layer’s transformation term contributes to the resnet’s prediction for x_n . The expression makes clear that the PredCP is performing functional regularization: a zero-favoring π_{KL} will encourage this variance to be small. Dropout has been shown to curb the variance of hidden units in a similar way [4]. Figure 3(b) shows

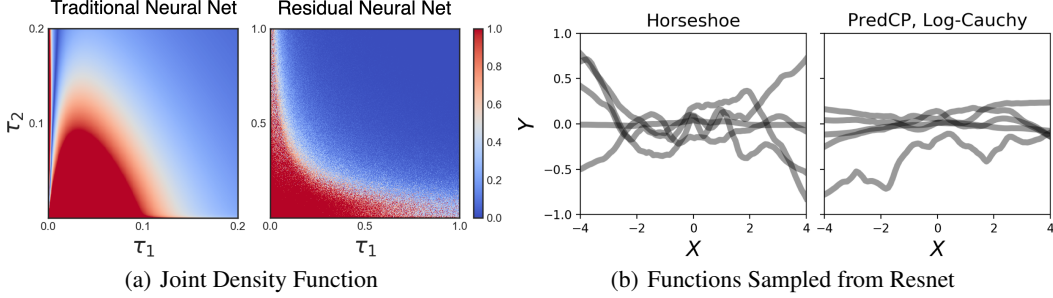


Figure 3: *Depth-Wise PredCP*. Subfigure (a) shows $\pi(\tau_1, \tau_2)$ for traditional (left) and residual (right) NNs. Subfigure (b) shows functions sampled from a resnet with a PredCP and a horseshoe prior for comparison. The KLD prior is Log-Cauchy(0, 1) in both cases.

functions sampled from a resnet with a horseshoe prior (left) and a depth-wise log-Cauchy PredCP (right). The PredCP’s samples are closer to linear due to the regularization of the predictive variance. Yet, recall that the log-Cauchy is heavy-tailed and therefore allows some functions to stray from the origin, as we see one sample has done.

Hierarchical Modeling for Meta-Learning Meta-learning is another natural application for the PredCP as it can control the degree to which information is pooled across tasks. Following the approach of Chen et al. [11], we use the generative model: $\mathcal{D}_t \sim p(\mathcal{D}_t | \theta_t)$, $\theta_t \sim N(\phi, \tau \mathbb{I})$ where t indexes the task, \mathcal{D}_t is data for the t th task, θ_t are local parameters specific to the t th task, and $\{\phi, \tau\}$ are global *meta-parameters*. The scale τ controls local adaptation, and as $\tau \rightarrow 0^+$, the task structure becomes irrelevant. This hierarchical meta-learning model is perfectly suited for a PredCP: the global parameters ϕ define the base model and the task-specific parameters θ_t define the extended model. The PredCP then controls task adaptation by comparing the predictions under local vs global parameters:

$$\pi(\tau) = \pi_{\text{KL}} \left(\frac{1}{T} \sum_{t=1}^T \mathbb{E}_{\theta_t | \tau} \text{KL} [p_+(\mathcal{D}_t | \theta_t) || p_0(\mathcal{D}_t | \phi)] \right) \left| \frac{1}{T} \sum_t \frac{\partial \mathbb{E}_{\theta_t | \tau} \text{KL}_t}{\partial \tau} \right| \quad (10)$$

where $\mathbb{E}_{\theta_t | \tau} \text{KL}_t$ is shorthand for the expected KLD on the t th task. In the experiments, we follow Chen et al. [11]’s modular specification by applying the PredCP layer-wise. Doing so allows the feature-extracting shallow layers to adapt to a different degree than the classification-based final layer.

6 Experiments

We evaluate the PredCP on regression, classification, and few-shot learning tasks under a variety of algorithms for posterior inference. The experimental details are provided in Appendices E, F, and G.

Logistic Regression We first report a smaller-scale experiment in which the ECP can be computed and posteriors obtained with high-fidelity. We use the logistic regression model: $y \sim \text{Bernoulli}(f(\mathbf{x}\beta))$, $\beta_d \sim N(0, \lambda_d^2 \tau^2)$, $\lambda_d \sim C^+(0, 1)$ where f denotes the logistic function and C^+ a half-Cauchy prior. We compare three priors for τ : $C^+(0, 1)$, which is the default prior recommended by Gelman [19] and Carvalho et al. [9], the ECP (via probit approximation [5]), and the PredCP. The log-Cauchy(0, 1) is the KLD prior. We use Stan [8] to obtain the full posterior $p(\beta, \lambda, \tau | \mathbf{X}, \mathbf{y})$, performing both variational inference (Normal mean-field approximation) [31] and Hamiltonian MC. We test the priors on three small medical data sets [21, 1, 41], two of which are high-dimensional (2000+), so that the prior strongly influences the posterior. Table 1 reports the predictive log-likelihood on the test set averaged over 20 splits. The ECP and PredCP have comparable performance and outperform the half-Cauchy in four of six cases and with one tie.

Neural Networks We next report results using resnets for regression: $y \sim N(y | \mathbf{x}, \{\mathbf{W}_l\}_{l=1}^3)$, $w_{l,i,j} \sim N(0, \lambda_{l,i}^2 \tau_l)$, $\lambda_{l,i} \sim \Gamma^{-1}(3, 3)$ where l indexes layers, i rows of the weight matrix, and j columns. This prior has two forms of Bayesian regularization. The row-wise scale $\lambda_{l,i}$ implements

Table 1: *Logistic Regression*. Below we report test set predictive log-likelihoods for the half-Cauchy prior, ECP, and PredCP under both VI and MCMC. Results are averaged across 20 splits.

DATA SET	N _{train}	D	VARIATIONAL INFERENCE			MARKOV CHAIN MONTE CARLO		
			HALF-CAUCHY	ECP	PREDCP	HALF-CAUCHY	ECP	PREDCP
allaml	51	7129	-0.43±.01	-0.32±.01	-0.32±.01	-0.19±.02	-0.17±.02	-0.17±.02
colon	44	2000	-0.61±.02	-0.63±.03	-0.66±.02	-0.54±.05	-0.52±.05	-0.54±.04
breast	82	9	-0.60±.01	-0.58±.01	-0.58±.01	-0.55±.02	-0.55±.01	-0.55±.02

automatic relevance determination (ARD) [35, 38], which controls the effective width. The layer-wise scale τ_l performs *automatic depth determination* (ADD) [37], as it controls the effective depth. We again compare three strategies for setting τ . The first is to use a fixed scale ($\tau = \tau_0$), thereby removing ADD and serving as a weak baseline. The second is to use a shrinkage prior. Nalisnick et al. [37] use an inverse gamma prior, and we report their results as the strong baseline. For our method we use the PredCP with a log-Cauchy(0, 1) KLD prior. For posterior inference, we use Bayes-by-backprop [6] for the weights and variational EM [56, 37] for the scales λ and τ . The maximization step cannot be performed analytically for the PredCP, as it can for the inverse Gamma, and so we perform iterative gradient-based optimization. Results on UCI benchmarks [13, 25] are reported in Table 2. Using the PredCP results in the best test set root-mean-square error (RMSE) for three of the seven benchmarks (boston, energy, yacht) and in one tie (kin8nm).

Table 2: *ARD-ADD Resnet*. Below we report test set RMSE for UCI benchmarks, comparing the PredCP against a shrinkage prior [37] and a fixed scale. Results are averaged across 20 splits.

Prior Type	boston	concrete	energy	kin8nm	power	wine	yacht
FIXED	2.29 ±.33	3.51 ±.41	0.83 ±.14	0.06 ±.00	3.32 ±.09	0.58 ±.04	0.66 ±.12
SHRINKAGE [37]	2.37 ±.18	3.76 ±.23	0.85 ±.08	0.06 ±.00	3.24 ±.07	0.54 ±.03	0.60 ±.16
PREDCP	2.26 ±.06	3.70 ±.46	0.82 ±.07	0.06 ±.00	3.27 ±.09	0.56 ±.03	0.57 ±.03

Few-Shot Learning Our final experiment evaluates the PredCP for few-shot learning. We follow Chen et al. [11]’s experimental framework, using the hierarchical model $\mathcal{D}_t \sim p(\mathcal{D}_t|\theta_t)$, $\theta_t \sim N(\phi, \tau\mathbb{I})$ (described in Section 5) and their σ -MAML algorithm for optimization. In essence, σ -MAML performs MAP estimation for θ_t , ϕ , and τ . The classifier is the standard four-layer convolutional NN [14]. We experimentally compare four different priors, each applied layer-wise (again following Chen et al. [11]). The first baseline is $\theta_t \sim \mathbb{1}$ (improper uniform), which corresponds to standard MAML [14]. The second baseline is Chen et al. [11]’s model, which uses the improper uniform prior for the meta-parameters: $\phi_l, \tau_l \sim \mathbb{1}$. For a third baseline, we extend Chen et al. [11]’s model by placing a shrinkage prior on τ_l , considering half-Cauchy, log-Cauchy, exponential, and gamma-exponential mixture distributions. Finally, our proposal is to place a PredCP on τ_l . We use the same four shrinkage priors for π_{KL} . We evaluate all priors on the few-shot CIFAR100 [39] and mini-ImageNet [53] classification benchmarks, using the standard 5-way 1-shot and 5-shot protocols. Table 3 reports the results. The PredCP consistently improves accuracy across all experiments.

Table 3: *Few-Shot Learning*. Below we report test set accuracy for the PredCP, comparing it to a shrinkage prior, a uniform prior, and non-Bayesian MAML.

	FEWSHOT-CIFAR100		MINI-IMAGENET	
	1-SHOT	5-SHOT	1-SHOT	5-SHOT
MAML	35.6 ± 1.8	50.3 ± 0.9	46.8 ± 1.9	58.4 ± 0.9
σ -MAML + uniform prior [11]	39.3 ± 1.8	51.0 ± 1.0	47.7 ± 0.7	60.1 ± 0.8
σ -MAML + shrinkage prior	40.9 ± 1.9	52.7 ± 0.9	48.5 ± 1.9	60.9 ± 0.7
σ -MAML + PREDCP	41.2 ± 1.8	52.9 ± 0.9	49.3 ± 1.8	61.9 ± 0.9

7 Conclusions

We proposed a novel prior termed the *Predictive Complexity Prior* (PredCP). This prior is constructed procedurally and provides functional regularization. We experimentally demonstrated the PredCP’s utility, showing it improves predictive performance across a range of models, tasks, and inference strategies. We found the log-Cauchy(0, 1) to be a good default KLD prior. One potential avenue for future work is to re-introduce predictive correlations into the divergence function, as these were lost when switching to the upper bound (Equation 6). The resulting resnet-PredCP could then account for more interesting local structure in the predictive function, not just its point-wise variance.

Acknowledgements

The authors thank James Allingham and Javier Antorán for helpful feedback on the manuscript. We are also grateful to Samsung Electronics for financial support.

References

- [1] Uri Alon, Naama Barkai, Daniel A. Notterman, Kurt Gish, Suzanne Ybarra, Daniel Mack, and Arnold J. Levine. Broad Patterns of Gene Expression Revealed by Clustering Analysis of Tumor and Normal Colon Tissues Probed by Oligonucleotide Arrays. In *Proceedings of the National Academy of Sciences*, 1999.
- [2] Javier Antorán, James Urquhart Allingham, and José Miguel Hernández-Lobato. Variational Depth Search in ResNets. *ICLR Workshop on Neural Architecture Search*, 2020.
- [3] Andrei Atanov, Arsenii Ashukha, Kirill Struminsky, Dmitriy Vetrov, and Max Welling. The Deep Weight Prior. In *Proceedings of the International Conference on Learning Representations*, 2019.
- [4] Pierre Baldi and Peter J. Sadowski. Understanding Dropout. In *Advances in Neural Information Processing Systems*, 2013.
- [5] Christopher M. Bishop. *Pattern Recognition and Machine Learning*. Springer, 2006.
- [6] Charles Blundell, Julien Cornebise, Koray Kavukcuoglu, and Daan Wierstra. Weight Uncertainty in Neural Networks. In *Proceedings of the 32nd International Conference on Machine Learning*, 2015.
- [7] George E. P. Box. Sampling and Bayes’ Inference in Scientific Modelling and Robustness. *Journal of the Royal Statistical Society: Series A*, 1980.
- [8] Bob Carpenter, Andrew Gelman, Matthew D. Hoffman, Daniel Lee, Ben Goodrich, Michael Betancourt, Marcus Brubaker, Jiqiang Guo, Peter Li, and Allen Riddell. Stan: A Probabilistic Programming Language. *Journal of Statistical Software*, 2017.
- [9] Carlos M. Carvalho, Nicholas G. Polson, and James G. Scott. Handling Sparsity via the Horseshoe. In *Proceedings of the 12th International Conference on Artificial Intelligence and Statistics*, 2009.
- [10] George Casella. An Introduction to Empirical Bayes Data Analysis. *The American Statistician*, 1985.
- [11] Yutian Chen, Abram L. Friesen, Feryal Behbahani, David Budden, Matthew W. Hoffman, Arnaud Doucet, and Nando de Freitas. Modular Meta-Learning with Shrinkage. *NeurIPS Workshop on Meta-Learning*, 2019.
- [12] Georgi Dikov and Justin Bayer. Bayesian Learning of Neural Network Architectures. In *Proceedings of the 22nd International Conference on Artificial Intelligence and Statistics*, 2019.
- [13] Dheeru Dua and Casey Graff. UCI Machine Learning Repository, 2019.
- [14] Chelsea Finn, Pieter Abbeel, and Sergey Levine. Model-Agnostic Meta-Learning for Fast Adaptation of Deep Networks. In *Proceedings of the 34th International Conference on Machine Learning*, 2017.
- [15] Daniel Flam-Shepherd, James Requeima, and David Duvenaud. Mapping Gaussian Process Priors to Bayesian Neural Networks. *NeurIPS Workshop on Bayesian Deep Learning*, 2017.

- [16] Daniel Flam-Shepherd, James Requeima, and David Duvenaud. Characterizing and Warping the Function Space of Bayesian Neural Networks. *NeurIPS Workshop on Bayesian Deep Learning*, 2018.
- [17] Geir-Arne Fuglstad, Daniel Simpson, Finn Lindgren, and Håvard Rue. Constructing Priors that Penalize the Complexity of Gaussian Random Fields. *Journal of the American Statistical Association*, 2019.
- [18] Yarin Gal and Zoubin Ghahramani. Dropout as a Bayesian Approximation: Representing Model Uncertainty in Deep Learning. In *Proceedings of the 33rd International Conference on Machine Learning*, 2016.
- [19] Andrew Gelman. Prior Distributions for Variance Parameters in Hierarchical Models. *Bayesian Analysis*, 2006.
- [20] Andrew Gelman, Daniel Simpson, and Michael Betancourt. The Prior Can Often Only Be Understood in the Context of the Likelihood. *Entropy*, 2017.
- [21] Todd R. Golub, Donna K. Slonim, Pablo Tamayo, Christine Huard, Michelle Gaasenbeek, Jill P. Mesirov, Hilary Coller, Mignon L. Loh, James R. Downing, and Mark A. Caligiuri. Molecular Classification of Cancer: Class Discovery and Class Prediction by Gene Expression Monitoring. *Science*, 1999.
- [22] Danijar Hafner, Dustin Tran, Timothy Lillicrap, Alex Irpan, and James Davidson. Noise Contrastive Priors for Functional Uncertainty. In *Proceedings of the 35th Conference on Uncertainty in Artificial Intelligence*, 2019.
- [23] Kaiming He, Xiangyu Zhang, Shaoqing Ren, and Jian Sun. Deep Residual Learning for Image Recognition. In *Proceedings of the IEEE Conference on Computer Vision and Pattern Recognition*, 2016.
- [24] Jonathan Heck and Nal Kalchbrenner. Bayesian Inference for Large Scale Image Classification. *ArXiv e-Prints*, 2019.
- [25] José Miguel Hernández-Lobato and Ryan Adams. Probabilistic Backpropagation for Scalable Learning of Bayesian Neural Networks. In *Proceedings of the 32nd International Conference on Machine Learning*, 2015.
- [26] Harold Jeffreys. An Invariant Form for the Prior Probability in Estimation Problems. In *Proceedings of the Royal Society of London A: Mathematical, Physical and Engineering Sciences*, 1946.
- [27] Valen E. Johnson and David Rossell. On the Use of Non-Local Prior Densities in Bayesian Hypothesis Tests. *Journal of the Royal Statistical Society: Series B*, 2010.
- [28] Diederik Kingma and Jimmy Ba. Adam: A Method for Stochastic Optimization. In *Proceedings of the International Conference on Learning Representations*, 2014.
- [29] Diederik Kingma and Max Welling. Efficient Gradient-Based Inference Through Transformations Between Bayes Nets and Neural Nets. In *Proceedings of the 31st International Conference on Machine Learning*, 2014.
- [30] Nadja Klein and Thomas Kneib. Scale-Dependent Priors for Variance Parameters in Structured Additive Distributional Regression. *Bayesian Analysis*, 2016.
- [31] Alp Kucukelbir, Dustin Tran, Rajesh Ranganath, Andrew Gelman, and David Blei. Automatic Differentiation Variational Inference. *The Journal of Machine Learning Research*, 2017.
- [32] Christos Louizos, Xiahao Shi, Klamer Schutte, and Max Welling. The Functional Neural Process. In *Advances in Neural Information Processing Systems*, 2019.
- [33] Chao Ma, Yingzhen Li, and José Miguel Hernández-Lobato. Variational Implicit Processes. In *Proceedings of the 36th International Conference on Machine Learning*, 2019.
- [34] Fangchang Ma, Ulas Ayaz, and Sertac Karaman. Invertibility of Convolutional Generative Networks from Partial Measurements. In *Advances in Neural Information Processing Systems*, 2018.
- [35] David MacKay. Bayesian Non-Linear Modeling for the Prediction Competition. *Maximum Entropy and Bayesian Methods*, 1994.
- [36] Eric Nalisnick and Padhraic Smyth. Learning Priors for Invariance. In *Proceedings of the 21st International Conference on Artificial Intelligence and Statistics*, 2018.

- [37] Eric Nalisnick, José Miguel Hernández-Lobato, and Padhraic Smyth. Dropout as a Structured Shrinkage Prior. In *Proceedings of the 36th International Conference on Machine Learning*, 2019.
- [38] Radford M. Neal. *Bayesian Learning for Neural Networks*. PhD thesis, University of Toronto, 1994.
- [39] Boris Oreshkin, Pau Rodríguez López, and Alexandre Lacoste. TADAM: Task Dependent Adaptive Metric for Improved Few-Shot Learning. In *Advances in Neural Information Processing Systems*, 2018.
- [40] George Papamakarios, Eric Nalisnick, Danilo Jimenez Rezende, Shakir Mohamed, and Balaji Lakshminarayanan. Normalizing Flows for Probabilistic Modeling and Inference. *ArXiv e-Prints*, 2019.
- [41] Miguel Patrício, José Pereira, Joana Crisóstomo, Paulo Matafome, Manuel Gomes, Raquel Seça, and Francisco Caramelo. Using Resistin, Glucose, Age and BMI to Predict the Presence of Breast Cancer. *BMC Cancer*, 2018.
- [42] Tim Pearce, Russell Tsuchida, Mohamed Zaki, Alexandra Brintrup, and Andy Neely. Expressive Priors in Bayesian Neural Networks: Kernel Combinations and Periodic Functions. In *Proceedings of the 35th Conference on Uncertainty in Artificial Intelligence*, 2019.
- [43] Mary Phuong and Christoph H. Lampert. Functional vs. Parametric Equivalence of ReLU Networks. In *Proceedings of the International Conference on Learning Representations*, 2020.
- [44] Juho Piironen and Aki Vehtari. On the Hyperprior Choice for the Global Shrinkage Parameter in the Horseshoe Prior. In *Proceedings of the 20th International Conference on Artificial Intelligence and Statistics*, 2017.
- [45] Christian Robert. *The Bayesian Choice*. Springer, 2001.
- [46] Minsuk Shin, Anirban Bhattacharya, and Valen E. Johnson. Scalable Bayesian Variable Selection Using Nonlocal Prior Densities in Ultrahigh-Dimensional Settings. *Statistica Sinica*, 2018.
- [47] Daniel Simpson, Håvard Rue, Andrea Riebler, Thiago G. Martins, and Sigrunn H. Sørbye. Penalising Model Component Complexity: A Principled, Practical Approach to Constructing Priors. *Statistical Science*, 2017.
- [48] Yang Song, Chenlin Meng, and Stefano Ermon. MintNet: Building Invertible Neural Networks with Masked Convolutions. In *Advances in Neural Information Processing Systems*, 2019.
- [49] Sigrunn Holbek Sørbye and Håvard Rue. Penalised Complexity Priors for Stationary Autoregressive Processes. *Journal of Time Series Analysis*, 2017.
- [50] Shengyang Sun, Guodong Zhang, Jiaxin Shi, and Roger Grosse. Functional Variational Bayesian Neural Networks. In *Proceedings of the International Conference on Learning Representations*, 2019.
- [51] Massimo Ventrucci and Håvard Rue. Penalized Complexity Priors for Degrees of Freedom in Bayesian P-Splines. *Statistical Modelling*, 2016.
- [52] Massimo Ventrucci, Daniela Cocchi, Gemma Burgazzi, and Alex Laini. PC Priors for Residual Correlation Parameters in One-Factor Mixed Models. *Statistical Methods & Applications*, 2019.
- [53] Oriol Vinyals, Charles Blundell, Tim Lillicrap, and Daan Wierstra. Matching Networks for One Shot Learning. In *Advances in Neural Information Processing Systems*, 2016.
- [54] Yeming Wen, Paul Vicol, Jimmy Ba, Dustin Tran, and Roger Grosse. Flipout: Efficient Pseudo-Independent Weight Perturbations on Mini-Batches. In *Proceedings of the International Conference on Learning Representations*, 2018.
- [55] Florian Wenzel, Kevin Roth, Bastiaan S. Veeling, Jakub Świątkowski, Linh Tran, Stephan Mandt, Jasper Snoek, Tim Salimans, Rodolphe Jenatton, and Sebastian Nowozin. How Good is the Bayes Posterior in Deep Neural Networks Really? In *Proceedings of the 37th International Conference on Machine Learning*, 2020.
- [56] Anqi Wu, Sebastian Nowozin, Edward Meeds, Richard E. Turner, José Miguel Hernández-Lobato, and Alexander L. Gaunt. Deterministic Variational Inference for Robust Bayesian Neural Networks. In *Proceedings of the International Conference on Learning Representations*, 2019.

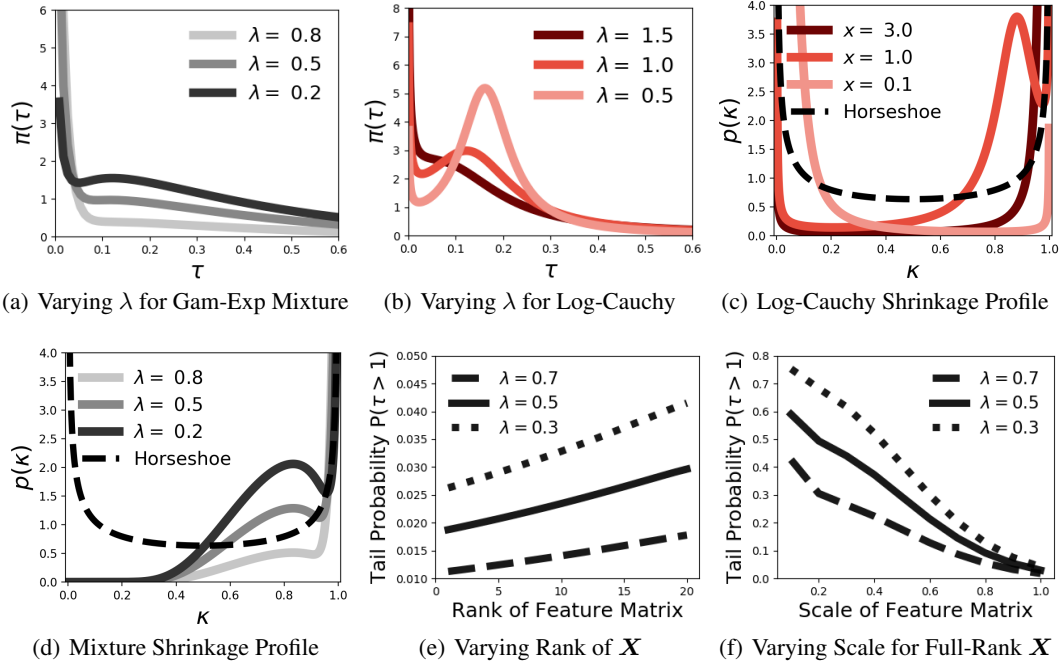


Figure 4: $\pi(\tau)$ for *Linear Regression*. Subfigures 4(a) and 4(b) show how the mixture and log-Cauchy ECP for τ changes as a function of λ . Subfigures 4(c) and 4(d) show the shrinkage profiles for the log-Cauchy and mixture ECPs (respectively). Subfigures 4(e) and 4(f) show how varying the rank and scale of the design matrix affects the ECP’s tail probability.

- [57] A. Zellner. On Assessing Prior Distributions and Bayesian Regression Analysis with g-Prior Distributions. *Bayesian Inference and Decision Techniques*, 1986.
- [58] Ruqi Zhang, Chunyuan Li, Jianyi Zhang, Changyou Chen, and Andrew Gordon Wilson. Cyclical Stochastic Gradient MCMC for Bayesian Deep Learning. In *Proceedings of the International Conference on Learning Representations*, 2020.

A ECP for Linear Regression, continued

A.1 Varying Prior Parameters

We consider the following priors on the KLD, denoted π_{KL} in the main text:

- Exponential($x; \lambda$) = $e^{-x/\lambda}/\lambda$
- Gamma($x; \lambda = \{\lambda_1, \lambda_2\}$) = $\frac{x^{\lambda_1-1}}{\Gamma(\lambda_1)\lambda_2} e^{-x/\lambda_2}$
- Log-Cauchy($x; \lambda$) = $\frac{1}{\pi x} \left(\frac{\lambda}{(\log x)^2 + \lambda^2} \right)$

Since the gamma prior favors p_0 and the exponential p_+ , we also consider a mixture of the two:

$$\pi(\text{KL}; \lambda) = \lambda \text{Gamma}(\text{KL} [p_+ || p_0]) + (1 - \lambda) \text{Exponential}(\text{KL} [p_+ || p_0]).$$

This mixture should achieve the same interpolation behavior as the log-Cauchy, balancing preferences for p_0 and p_+ . See Figure 4(a) for a visualization of the ECP for the gamma-exponential mixture as the mixing coefficient is varied. Figure 4(b) shows the log-Cauchy ECP as its scale is varied.

A.2 Dynamic Shrinkage Profile

One method for illuminating and comparing the effects of shrinkage priors is through their corresponding *shrinkage profile* [9]. Consider the model: $y \sim \text{N}(\theta, 1)$, $\theta \sim \text{N}(0, \tau)$, $\tau \sim p(\tau)$. Given one observation $y = y_0$, the Bayes estimator for θ is: $\mathbb{E}[\theta | y_0, \tau] = \kappa \cdot 0 + (1 - \kappa) \cdot y_0$, $\kappa = 1/(1 + \tau)$.

Making the change of variables $p(\kappa) = p(\tau) \left| \frac{d}{d\kappa} 1/\kappa - 1 \right|$, we can examine the induced prior $p(\kappa)$. If $p(\kappa)$ places high density near $\kappa = 1$, then the prior provides strong regularization since the Bayes estimator would be near zero. Conversely, a strong mode at $\kappa = 0$ means the resulting estimator would be near y_0 , implying a tendency to follow the data. Figure 4(c) shows the shrinkage profile for the log-Cauchy ECP for $x \in \{.1, 1, 3\}$, comparing the profiles of the horseshoe’s. The horseshoe is an effective prior for robust regression since it is designed to equally favor 0 and 1 ($\kappa \sim \text{Beta}(.5, .5)$). The shrinkage profile for the log-Cauchy also can place density at both extremes. However, unlike the horseshoe, the ECP enables *dynamic* shrinkage, being able to adjust the profile as a function of x . We see that for $x = 0.1$, the log-Cauchy ECP actually favors the unshrunk solution whereas for $x = 3$ strong shrinkage is preferred. The mixture ECP’s shrinkage profile is shown in Figure 4(d). Due to the exponential not having a heavy tail, the mixture ECP’s profile cannot place any significant density at $\kappa = 0$, meaning that the model can never completely ‘forget’ the shrinkage regularization.

A.3 Example: Multivariate Regression

We now examine the case of multivariate regression: $\mathbb{E}[\mathbf{y}|\mathbf{X}, \boldsymbol{\beta}] = \mathbf{X}\boldsymbol{\beta}$, where $\mathbf{y} \in \mathbb{R}^N$ is an N -dimensional vector of responses, $\mathbf{X} \in \mathbb{R}^{N \times D}$ the design matrix, and $\boldsymbol{\beta} \in \mathbb{R}^D$ a vector of parameters. Using the multivariate analogs of the priors from above— $p_0 = \delta(|\boldsymbol{\beta} - \mathbf{0}|)$, $p_+ = \text{N}(\mathbf{0}, \tau\mathbb{I})$ —we can derive the following ECP:

$$\pi(\tau; \boldsymbol{\lambda}, \mathbf{X}) = \pi_{\text{KL}} \left(\frac{-1}{2} \log |\mathbb{I} + \tau \sigma_y^{-2} \mathbf{X}^T \mathbf{X}| + \frac{\tau}{2\sigma_y^2} \text{tr} \{ \mathbf{X}^T \mathbf{X} \}; \boldsymbol{\lambda} \right) \left| \frac{\partial \text{KL}}{\partial \tau} \right| \quad (11)$$

where $\text{tr}\{\cdot\}$ denotes the trace operation and $|\cdot|$ the determinant. The KLD is computed between $p_+(\mathbf{y}|\mathbf{X}, \tau)$ and $p_0(\mathbf{y}|\mathbf{X})$. We omit the details of the volume term due to space constraints.

Here the KLD is a multidimensional integral that takes into account *correlations* in the model’s predictions. Hence, we can explore how characteristics of the design matrix influence the prior. We consider the tail probability $P(\tau > 1)$ since, as probability mass moves away from the origin, the ECP increasingly prefers the extended model. Below we describe simulations using the mixture ECP due to its mixing weight λ being interpretable. First consider the case in which \mathbf{X} has a rank of one and all row vectors have a length of one. This means that the data is essentially redundant, generating the same predictions. As the rank of \mathbf{X} increases, the predictions start to become varied and the model output becomes responsive to each x_n . Thus, we should expect $\pi(\tau)$ to favor larger values as the rank of \mathbf{X} increases. Indeed, this is exactly the behavior we observe in Figure 4(e), plotting the tail probability $P(\tau > 1)$ as we vary the rank from 1 to 20. Another attribute of \mathbf{X} we can vary is its scale: $\alpha\mathbf{X}$. Subfigure 4(f) shows the tail probability as the scale α increases (for full-rank \mathbf{X}). We find that scale changes result in more pronounced tail effects than changes in rank.

A.4 Example: ECP for the Linear Regression Coefficient

In the main text, we consider applying the ECP to the scale of the prior on $\boldsymbol{\beta}$, the regression coefficients. Yet, we can also define the ECP on $\boldsymbol{\beta}$ directly. Consider the linear model $\mathbb{E}[y|x, \boldsymbol{\beta}] = \beta_0 + \beta_1 x$, $\beta_0 \sim \text{N}(0, \sigma_{\beta_0}^2)$. We wish to define the ECP on β_1 to control deviation from the base model $p_0 : \beta_1 = 0$:

$$\begin{aligned} \pi(\beta_1; \lambda, x) &= \pi_{\text{KL}} (\text{KL} [p_+(y|x, \beta_1) || p_0(y|x)]; \lambda) \left| \frac{\partial \text{KL} [p_+(y|x, \beta_1) || p_0(y|x)]}{\partial \beta_1} \right| \\ &= \frac{1}{2} \pi_{\text{KL}} \left(\frac{\beta_1^2 x^2}{2(\sigma_y^2 + \sigma_{\beta_0}^2)}; \lambda \right) \left| \frac{\beta_1 x^2}{\sigma_y^2 + \sigma_{\beta_0}^2} \right| \end{aligned} \quad (12)$$

where σ_y^2 is the response noise. Figure 5(a) shows three choices for π_{KL} —exponential (green), gamma (purple), and log-Cauchy (red)—and Figure 5(b) shows the prior each induces on β_1 . We see that choice of π_{KL} is significant. If π_{KL} places too little density at zero, the volume term $|\beta_1 x^2 / (\sigma_y^2 + \sigma_{\beta_0}^2)|$ in the ECP dominates, driving $\pi(\beta_1)$ to zero at $\beta_1 = 0$. In turn, this drives β_1 from reflecting the behavior of p_0 and suppresses any regularization. We see this behavior from the exponential (green) as its ECP has no density at zero. At the other end of the spectrum is the gamma (purple). It places too much density at zero, forcing $\pi(\beta_1)$ to preference the base model $\beta_1 = 0$. Lastly, the log-Cauchy (red) has the most interesting behavior: it has strong shrinkage at the origin to reflect p_0 but also significant density away from zero to represent p_+ . Hence the log-Cauchy is able to balance preferences for both p_+ and p_0 , interpolating between the exponential and gamma’s single-mindedness. Lastly, Figure

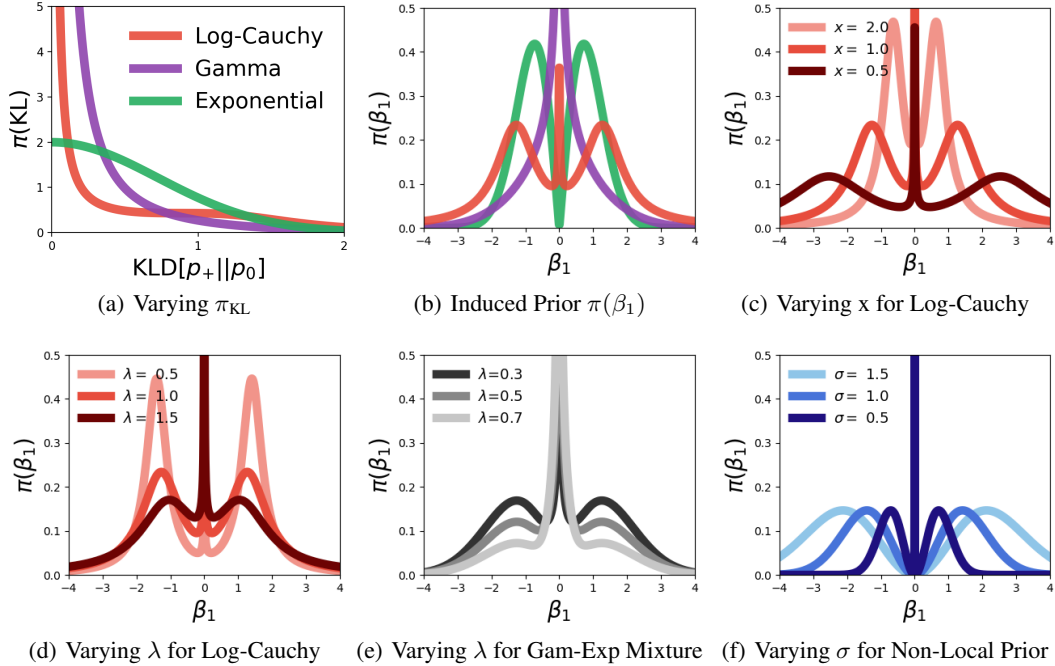


Figure 5: $\pi(\beta_1)$ for *Linear Regression*. Subfigure 5(a) shows three choices for π_{KL} : exponential ($\lambda = .5$), gamma ($\lambda = (.2, 2)$), and log-Cauchy ($\lambda = 1$). Subfigure 5(b) shows the priors induced on β_1 for each KLD prior. Subfigure 5(c) shows how the log-Cauchy ECP changes as a function of x . Subfigure 5(d) shows how the log-Cauchy ECP changes when varying its scale parameter ($x = 1$). Subfigure 5(e) shows how the mixture (gamma and exponential) ECP changes when varying the mixture weight λ ($x = 1$). Subfigure 5(f) shows the non-local prior for three scales.

5(c) shows how $\pi(\beta_1)$ changes as x is varied—the data adaptive nature mentioned above. The ECP’s shrinkage is adjusted to the scale of the features, applying stronger regularization when x is large and relaxing as x decreases. This is sensible since the models predictions cannot change as drastically for small x s as they can for large x s.

Connection to Non-Local Priors Perhaps the (log-Cauchy and mixture) ECP’s most interesting feature is in how it balances between p_0 and p_+ through multi-modality. In addition to the strong mode at zero, there are modes separated from and symmetric about the origin; see Figure 5(d). This is the defining feature of so-called *non-local priors* [27]. This class of priors is designed to achieve good convergence rates in Bayesian hypothesis testing by carefully allocating density exactly at the null and distinctly away from the null to represent the alternative. Shin et al. [46] apply this non-local principle to Bayesian variable selection in high-dimensional regression via the following prior:

$$\beta \sim z\delta_0 + (1 - z)p_{\text{NL}}(\beta), \quad z \sim \text{Bernoulli}(\rho), \quad p_{\text{NL}}(\beta) = \frac{\beta^2}{\sigma} \text{N}(\beta; 0, \sigma) \quad (13)$$

where β is the linear model’s coefficient and p_{NL} is known as a *product (2nd) moment prior* [27]. See Figure 5(f) for a visualization. While the ECP and non-local prior have clear similarities, the connection can be made explicit by considering the Bayes factor $\text{BF}(+|0) = p_+(y|\mathbf{x}, \theta_+)/p_0(y|\mathbf{x})$, which is what we would use to test $H_0 : \theta_+ = 0$ vs $H_1 : \theta_+ \neq 0$. The ECP’s KLD term contains this exact expression: $\text{KL}[p_+ || p_0] = \mathbb{E}_{p_+}[\log \text{BF}(+|0)]$, which can be interpreted as the (log) Bayes factor expected if the data is truly generated by the extended model.

B Bijectivity Conditions for Neural Networks

Below we show that $\mathbb{E}_{\theta|\tau} \text{KL}[p_+ || p_0]$ is bijective w.r.t. τ for Gaussian and categorical observation models, ReLU activations, and Gaussian weight priors $\mathbf{W}_l \sim \text{N}(\Phi_l, \tau_l \Sigma)$. We assume the base model has weights $\mathbf{W}_l \sim \delta[\Phi_l]$, where Φ_l is the prior mean of the expanded model. In turn, the

change of variables is well-defined and the PredCP is proper (i.e. integrates to 1) when used in the applications given in Section 5. Before diving into the technical details, we point out that invertibility should not be hard to guarantee since $\tau \in \mathbb{R}^+$ is a scalar. If the reader is familiar with the literature on *normalizing flows* [40] and invertible architectures [48], one may have the impression that invertibility is hard to guarantee for neural networks, often requiring constraints on the weights. This is only the case because an invertible architecture must preserve bijectivity w.r.t. the entire input *vector*. We, to the contrary, just have to preserve scalar information. Moreover, we know this scalar τ is strictly positive, which eliminates any symmetry about the origin. Thus, intuitively, the information about τ should be preserved at every hidden layer as long as at least one ReLU unit is active. This brings up the only assumption that we require: *non-degeneracy*. That is, for every hidden layer, there must be at least one active ReLU unit (i.e. a unit evaluated to a positive value). This is an extremely weak assumption, especially for all but the smallest neural networks, and ReLU networks commonly satisfy much stronger non-degeneracy assumptions [43]. If dead layers would arise for some reason, initializing the biases to be positive should prevent the pathology. Before moving on to the main results, we first introduce two conventions.

Non-Centered Parameterization: We assume all weights are represented in the observation model $p(\mathbf{y}|\mathbf{X}, \mathbf{W})$ using the following non-centered form: $\mathbf{W}_l \stackrel{d}{=} \Phi_l + \sqrt{\tau_l} \cdot \Xi_l$, $\Xi_l \sim \mathcal{N}(\mathbf{0}, \Sigma)$. This parameterization is useful for ‘exposing’ τ_l so that we can write the KLD as an explicit function of τ .

Linear Representation of ReLU Activations Recall that feedforward networks with ReLU activations are piecewise-linear functions. Thus, it is equivalent to express a dense ReLU layer in terms of a diagonal ‘gating’ matrix $\tilde{\mathbb{I}}$ [34]:

$$\text{ReLU}(\mathbf{h}\mathbf{W}) = \mathbf{h}\mathbf{W}\tilde{\mathbb{I}}, \quad \text{where } \tilde{i}_{j,j} = 1 \text{ if } 0 < \sum_{i=1}^D w_{i,j}h_i, \quad (14)$$

otherwise $\tilde{i}_{j,j} = 0$. Using this convention, we can then represent the network’s linear output as:

$$\mathbf{F}_{out} = \mathbf{X} \left(\prod_{l=1}^L \mathbf{W}_l \tilde{\mathbb{I}}_l \right) \mathbf{W}_{out}$$

where \mathbf{F}_{out} is a matrix containing the network’s linear output (i.e. before a softmax is applied, in the classification setting) for all training features \mathbf{X} .

B.1 Gaussian Observation Model

Let’s now consider checking for bijectivity w.r.t. τ_l when the observation model is Gaussian, i.e. $\mathbf{y} \sim \mathcal{N}(\mathbf{f}_{out}, \sigma_y^2 \mathbb{I})$. The expected KLD is then:

$$\begin{aligned} \mathbb{E}_{\mathbf{W}_l|\tau_l} \text{KL}[\mathcal{N}(\mathbf{F}_{out}^+, \sigma_y^2 \mathbb{I}) || \mathcal{N}(\mathbf{F}_{out}^0, \sigma_y^2 \mathbb{I})] &= \frac{1}{2\sigma_y^2} \sum_{n=1}^N \sum_{d=1}^D \mathbb{E}_{\mathbf{W}_l|\tau_l} \left[\left(f_{n,d,out}^+ - f_{n,d,out}^0 \right)^2 \right] \\ &= \frac{1}{2\sigma_y^2} \sum_{n=1}^N \sum_{d=1}^D \mathbb{E}_{\mathbf{W}_l|\tau_l} \left[(f_{n,d,out}^+)^2 \right] - 2\mathbb{E}_{\mathbf{W}_l|\tau_l} [f_{n,d,out}^+] f_{n,d,out}^0 + (f_{n,d,out}^0)^2 \end{aligned} \quad (15)$$

where n indexes the training features and d the output dimensions. Since f_{out}^0 does not involve τ_l , we can treat it as a constant. The sum over n and d forms a conic combination. Therefore if all terms have the same monotonicity and are bijective, then the sum will be bijective as well.

We first turn toward the expectation in the middle term and expand it using the non-centered parameterization. We drop the indexes to help with notational clutter:

$$\begin{aligned} \mathbb{E}_{\mathbf{W}_l|\tau_l} [f_{out}^+] &= \mathbb{E}_{\mathbf{W}_l|\tau_l} \left[\mathbf{x} \left(\prod_{l=1}^L \tilde{\mathbb{I}}_l \mathbf{W}_l \right) \mathbf{w}_{out} \right] \\ &= \mathbb{E}_{\Xi_l} \left[\mathbf{x} \left(\prod_{l=1}^L (\Phi_l + \sqrt{\tau_l} \cdot \Xi_l) \tilde{\mathbb{I}}_l \right) \mathbf{w}_{out} \right] \\ &= \mathbb{E}_{\Xi_l} \left[\mathbf{x} \left(\prod_{l=1}^L \Phi_l \tilde{\mathbb{I}}_l \right) \mathbf{w}_{out} \right] + \mathbb{E}_{\Xi_l} \left[\mathbf{x} \left(\prod_{l=1}^L \sqrt{\tau_l} \cdot \Xi_l \tilde{\mathbb{I}}_l \right) \mathbf{w}_{out} \right]. \end{aligned} \quad (16)$$

Pushing through the expectation, we have:

$$= \mathbf{x} \left(\prod_{l=1}^L \Phi_l \mathbb{E}_{\Xi_l} [\tilde{\mathbb{I}}_l] \right) \mathbf{w}_{out} + \mathbf{x} \left(\prod_{l=1}^L \sqrt{\tau_l} \cdot \mathbb{E}_{\Xi_l} [\Xi_l \tilde{\mathbb{I}}_l] \right) \mathbf{w}_{out}.$$

Considering the first term, we have that $\mathbb{E}[\tilde{i}] = 1$ if $\sum_i \phi_{i,j} \mathbf{h}_i > 0$. For the second, $\mathbb{E}_{\Xi_l} [\Xi_l \tilde{\mathbb{I}}_l] = \mathbf{0}$. Thus, $\mathbb{E}_{\mathbf{w}_l | \tau_l} [f_{out}^+]$ reduces to the first term, and since this term depends only on the prior means, it is equivalent to the output of the base model:

$$\mathbb{E}_{\mathbf{w}_l | \tau_l} [f_{out}^+] = f_{out}^0. \quad (17)$$

Now turning to the other expectation term in Equation 15 and using the expansion from Equation 16, we have:

$$\begin{aligned} \mathbb{E}_{\mathbf{w}_l | \tau_l} [(f_{out}^+)^2] = & \mathbb{E}_{\Xi_l} \left[\left(\mathbf{x} \left(\prod_{l=1}^L \Phi_l \tilde{\mathbb{I}}_l \right) \mathbf{w}_{out} \right)^2 + 2 \left(\mathbf{x} \left(\prod_{l=1}^L \Phi_l \tilde{\mathbb{I}}_l \right) \mathbf{w}_{out} \right) \left(\mathbf{x} \left(\prod_{l=1}^L \sqrt{\tau_l} \cdot \Xi_l \tilde{\mathbb{I}}_l \right) \mathbf{w}_{out} \right) \right. \\ & \left. + \left(\mathbf{x} \left(\prod_{l=1}^L \sqrt{\tau_l} \cdot \Xi_l \tilde{\mathbb{I}}_l \right) \mathbf{w}_{out} \right)^2 \right]. \end{aligned}$$

The middle term drops out after taking the expectation. We are left with the two remaining terms:

$$\mathbb{E}_{\mathbf{w}_l | \tau_l} [(f_{out}^+)^2] = \underbrace{\mathbb{E}_{\Xi_l} \left[\left(\mathbf{x} \left(\prod_{l=1}^L \Phi_l \tilde{\mathbb{I}}_l \right) \mathbf{w}_{out} \right)^2 \right]}_{\gamma_1^{>0}} + \tau_l \cdot \prod_{l' \neq l} \tau_{l'} \cdot \underbrace{\mathbb{E}_{\Xi_l} \left[\left(\mathbf{x} \left(\prod_{l=1}^L \Xi_l \tilde{\mathbb{I}}_l \right) \mathbf{w}_{out} \right)^2 \right]}_{\gamma_2^{>0}}.$$

We use the variables γ_1 and γ_2 to denote these two terms from here forward. They have the following three properties that will come in handy below. Firstly, their values are strictly positive due to the square and non-degeneracy assumption ($\text{trace}\{\tilde{\mathbb{I}}_l\} \neq 0 \ \forall l$). We emphasize this by giving them the superscript > 0 . Secondly, we know their derivative w.r.t. τ_l is zero. This is true for γ_1 because it depends on τ_l only through $\tilde{\mathbb{I}}$ and therefore only through the sign function. For γ_2 , it does not depend on τ_l ; we have factored it out already. Thirdly, γ_1 and γ_2 are bounded w.r.t. τ_l . We know this in the former case because, again, τ_l controls only the ‘gates’ in $\tilde{\mathbb{I}}$ and Φ is bounded. The latter case is trivial due to γ_2 not being a function of τ_l . Now substituting back into Equation 15, we have

$$\begin{aligned} \mathbb{E}_{\mathbf{w}_l | \tau_l} [(f_{out}^+)^2] - 2\mathbb{E}_{\mathbf{w}_l | \tau_l} [f_{out}^+] f_{out}^0 + (f_{out}^0)^2 &= \gamma_1^{>0} + \tau_l \gamma_2^{>0} - 2f_{out}^0 f_{out}^0 + (f_{out}^0)^2 \\ &= \gamma_1^{>0} + \tau_l \gamma_2^{>0} - (f_{out}^0)^2. \end{aligned} \quad (18)$$

All that is left to do is to check for injectivity and surjectivity. For the former, we need to verify the derivative has a constant sign, and we find that:

$$\frac{\partial}{\partial \tau_l} (\mathbb{E}_{\mathbf{w}_l | \tau_l} [(f_{out}^+)^2] - 2\mathbb{E}_{\mathbf{w}_l | \tau_l} [f_{out}^+] f_{out}^0 + (f_{out}^0)^2) = \gamma_2^{>0}.$$

Clearly, the derivative is always positive, meaning the function is strictly increasing. Lastly, for surjectivity, it is sufficient to check that

$$\begin{aligned} \gamma_1^{>0} + \tau_l \gamma_2^{>0} - (f_{out}^0)^2 &\rightarrow 0^+ \quad \text{as } \tau_l \rightarrow 0^+ \\ \gamma_1^{>0} + \tau_l \gamma_2^{>0} - (f_{out}^0)^2 &\rightarrow \infty \quad \text{as } \tau_l \rightarrow \infty. \end{aligned}$$

As $\tau \rightarrow 0$, we have that $\gamma_1 \rightarrow (f_{out}^0)^2$, therefore causing the first and last terms to cancel. The remaining $\tau_l \gamma_2^{>0}$ term is then forced to zero simply by τ going to zero. As $\tau \rightarrow \infty$, the second term is sufficient for the full quantity to go to infinity since all other terms are bounded as a function of τ .

B.2 Categorical Observation Model

In the previous subsection, we showed that bijectivity is preserved at least up through the neural network’s linear output \mathbf{F}_{out}^+ . We now consider the case of a categorical observation model. This case is harder to show explicitly because the expectation cannot be pushed through to individual terms as we did above. Rather, we base the argument on the fact that compositions of bijections form a bijection. In particular, given that f_{out}^+ is bijective, we need the three following operations to preserve that bijectivity: $\mathbb{E}_{\Xi} \circ \text{KLD} \circ \text{softmax} \circ f_{out}^+(\tau)$.

First considering the softmax, the softmax function is defined as:

$$\pi_j = \frac{\exp\{\tau x_j\}}{\sum_{d=1}^D \exp\{\tau x_d\}}$$

where $x_j \in \mathbb{R}$, $\tau \in \mathbb{R}^+$, $0 < \pi_j < 1$, and $\sum_{d=1}^D \pi_d = 1$. We want to prove that the softmax is invertible w.r.t. the scale τ for fixed $\mathbf{x} = \{x_1, \dots, x_D\}$. Since τ is a scalar, it suffices that only one π_j need be invertible. Below we show bijectivity by showing injectivity and then surjectivity. We can show injectivity by examining the softmax’s derivative w.r.t. τ and showing it has a constant sign:

$$\pi_j'(\tau) = \underbrace{\pi_j}_{(+)} \underbrace{\left(x_j - \sum_{d=1}^D \pi_d x_d\right)}_{(+)\text{ or }(-)}$$

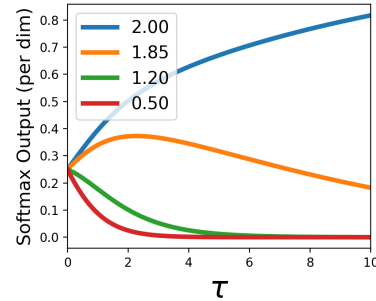
where the first term π_j is positive and the second could be positive or negative, depending on the \mathbf{x} values. Denoting the maximum element of \mathbf{x} as $x_{\max} = \max_d x_d$, the derivative in this dimension is:

$$\pi_{\max}'(\tau) = \underbrace{\pi_{\max}}_{(+)} \underbrace{\left(x_{\max} - \sum_{d=1}^D \pi_d x_d\right)}_{(+)} > 0,$$

and now we know the second term is strictly positive since $\sum_{d=1}^D \pi_d x_d$ is a convex combination of \mathbf{x} . That is, assuming that there’s at least one $x_d < x_{\max}$, then $\sum_{d=1}^D \pi_d x_d < x_{\max}$. Conversely, for $x_{\min} = \min_d x_d$, we have:

$$\pi_{\min}'(\tau) = \underbrace{\pi_{\min}}_{(+)} \underbrace{\left(x_{\min} - \sum_{d=1}^D \pi_d x_d\right)}_{(-)} < 0,$$

since $\sum_{d=1}^D \pi_d x_d > x_{\min}$. Thus, we have that at least two dimensions—those corresponding to x_{\min} and x_{\max} —of the softmax are injective w.r.t. τ . For surjectivity, it is sufficient to check the limits. For $\tau \rightarrow 0^+$, $\pi_j \rightarrow 1/D$ ($\forall j$), and for $\tau \rightarrow \infty$, we have $\pi_{\min} \rightarrow 0$ and $\pi_{\max} \rightarrow 1$. Thus, π_{\min} is strictly *decreasing* on $(1/D, 0)$ and that π_{\max} is strictly *increasing* on $(1/D, 1)$. In turn, $\text{Softmax}:\tau \mapsto \pi_{\min/\max}$ is a bijection. The figure to the right shows the softmax outputs for one particular setting of \mathbf{x} ; each line represents an output π_j . We see that the blue ($x = 2.00$) and red ($x = 0.50$) lines, the max and min dimensions respectively, are strictly monotonic. On the other hand, the orange line ($x = 1.85$) is clearly not bijective since it doesn’t pass the horizontal line test.



On to the KLD, $\text{KL}[p^+||p^0]$ is strictly convex w.r.t. p^+ for fixed p^0 . This is indeed our setting since only p^+ is a function of τ . This strict convexity implies that $\text{KL}[p^+||p^0]$ has a unique, global minimum at $\tau = 0$ and is strictly increasing as $\tau \rightarrow \infty$ —and hence, is bijective. Lastly, the expectation does not have an analytical solution, and thus here (as well as in practice), we consider the Monte Carlo approximation:

$$\mathbb{E}_{\Xi} \text{KL}[p(\mathbf{y}|\mathbf{X}, \Xi, \tau)||p_0(\mathbf{y}|\mathbf{X})] \approx \frac{1}{S} \sum_{s=1}^S \text{KL}[p(\mathbf{y}|\mathbf{X}, \hat{\Xi}_s, \tau)||p_0(\mathbf{y}|\mathbf{X})]$$

where the approximation becomes exact as $S \rightarrow \infty$. The Monte Carlo approximation is a weighted sum of bijective, strictly increasing functions and therefore is also strictly increasing and bijective.

B.3 Residual Networks

The preceding two sections hold as well for residual networks. In fact, residual networks allow us to relax the non-degeneracy assumption. That is, for invertibility w.r.t. τ_l , we can have $\mathbf{h}_j = \mathbf{0}$ for $j > l$ just so long as there is a path of skip (identity) connections from layer l to layer $m > j$. This identity path preserves the information about τ_l that would be lost due to $\mathbf{h}_j = \mathbf{0}$.

C Drawing Samples from the PredCP

The user may want to draw samples from the PredCP—for instance, to perform a prior predictive check [7]. In general, sampling from a reparameterized model can be done via: $\hat{x} \sim p(x)$, $\hat{\theta} = T(\hat{x})$ where $p(x)$ is the base distribution and T is the transformation [40]. Applying this formula to the PredCP, in theory, we could draw samples via:

$$\hat{\kappa} \sim \pi_{\text{KL}}, \quad \hat{\tau} = T^{-1}(\hat{\kappa}) \quad (19)$$

where $\hat{\kappa}$ represents a sampled value of $\mathbb{E}_{\theta|\tau} \text{KL}[p_+||p_0]$ and T^{-1} represents an inversion of the expected-KLD, yielding τ as a function of κ . Unfortunately, the analytical inverse of $\mathbb{E}_{\theta|\tau} \text{KL}[p_+||p_0]$ is not available in general. Instead, we use the numerical inversion technique proposed by Song et al. [48]. See Algorithm 1 below.

Algorithm 1 Sampling from the PredCP

Input: Prior $\pi_{\text{KL}}(\kappa)$, number of iterations T , step size α
Sample $\hat{\kappa} \sim \pi_{\text{KL}}(\kappa)$
Initialize $\tau_0 \leftarrow \hat{\kappa}$
For $t = [1, T]$:
 Compute $\mathbb{D}(\tau_{t-1}) = \mathbb{E}_{\theta|\tau_{t-1}} \text{KL}[p_+||p_0]$
 Compute $\partial \mathbb{D}(\tau_{t-1}) / \partial \tau_{t-1}$
 Update $\tau_t \leftarrow \tau_{t-1} - \alpha (\partial \mathbb{D}(\tau_{t-1}) / \partial \tau_{t-1})^{-1} (\mathbb{D}(\tau_{t-1}) - \hat{\kappa})$
Return τ_T

We used Algorithm 1 to sample from the depth-wise PredCP (described in Section 5) and ancestral sampling to draw functions from the NN. We considered both residual and non-residual architectures, both having batch normalization applied at each hidden layer. The observation model is Gaussian with $\sigma_y = 1$. We used a log-Cauchy(0, 1) KLD prior, $\alpha = 5 \times 10^{-5}$, $T = 20$, and 5 Monte Carlo samples for the $\theta|\tau$ expectation. In Figure 6, we show 5 function samples for the standard Normal, horseshoe ($\tau \sim C^+(0, 1)$), and PredCP for 5 and 25 hidden layers. The PredCP’s samples are notably simpler.

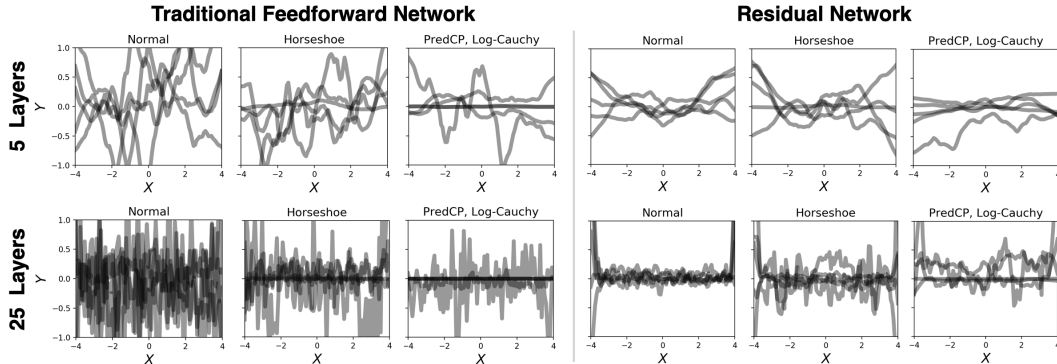


Figure 6: *Induced Prior Over Functions.* We compare a standard normal prior, the horseshoe ($\tau \sim C^+(0, 1)$), and the depth-wise PredCP ($\pi_{\text{KL}} = \text{Log-Cauchy}(0, 1)$) for 5 and 25 layer NNs.

D Modular Prior Specification for Meta-Learning

We provide details for specifying and evaluating *modular* priors for meta-learning. Following Chen et al. [11], we split θ into M distinct modules (e.g., layers), such that $\theta = [\theta_1^T, \dots, \theta_M^T]^T$. Our goal is then to place a separate prior on each module, and allow the modules to adapt differently to new tasks. Denoting ϕ_m and τ_m as the global parameters and shrinkage parameter of module m , respectively, we have that $\theta_{t,m} \sim \mathcal{N}(\phi_m, \tau_m \mathbb{I})$ for the local parameters of task t at module m . By specifying $p_m(\tau_m)$, we can control how much each module is allowed to deviate from the global model. For example, Chen et al. [11] place an improper flat prior on τ_m and perform MAP estimation. Importantly, to perform MAP estimation for $\{\tau_m\}_{m=1}^M$, we need only evaluate the log density of the priors $p_m(\tau_m)$, and add these terms to the outer-loop optimization objective [11].

Defining a PredCP Prior for τ In this setting, it is natural to consider the global parameters as defining the base model for the PredCP prior. We can achieve this by specifying the prior to be $p_{0,m}(\theta_{t,m}) = \delta(\theta_{t,m} - \phi_m)$. Denoting $p_0(\theta) = \prod_{m=1}^M p_{0,m}(\theta_m)$, we then have

$$p_0(\mathbf{y}|\mathbf{x}) = \int p(\mathbf{y}|\mathbf{x}, \theta) p_0(\theta) d\theta = p_\phi(\mathbf{y}|\mathbf{x}),$$

where we denote $p_\phi(\mathbf{y}|\mathbf{x})$ as the predictions made by the model using only global parameters. Next, for every module m , we can define the extended model

$$p_m(\mathbf{y}|\mathbf{x}, \tau_m) = \int p(\mathbf{y}|\mathbf{x}, \phi, \theta_m) p_m(\theta_m|\tau_m) d\theta_m,$$

where we use the notation $p(\mathbf{y}|\mathbf{x}, \phi, \theta_m)$ to denote the model that uses ϕ for all but module m , which uses θ_m . Using the notation from the main text, we further denote $p_0(D_t) = \prod_{\mathbf{x}, \mathbf{y} \in D_t} p_0(\mathbf{y}|\mathbf{x})$ and $p_m(D_t|\theta_{t,m}) = \prod_{\mathbf{x}, \mathbf{y} \in D_t} p_m(\mathbf{y}|\mathbf{x}, \phi, \theta_m)$. Recall that using the KLD upper bound, the PredCP prior for this setting can be expressed as

$$\pi(\tau_m) = \pi_{\text{KL}} \left(\frac{1}{T} \sum_{t=1}^T \mathbb{E}_{\theta_{t,m}|\tau_m} \text{KL} [p_m(D_t|\theta_{t,m}) || p_0(D_t)] \right) \left| \frac{1}{T} \sum_t \frac{\partial \mathbb{E}_{\theta_t|\tau} \text{KL}_t}{\partial \tau} \right|.$$

We can approximate the intractable term inside π_{KL} without bias via Monte-Carlo sampling:

$$\mathbb{E}_{\theta_{t,m}|\tau_m} \text{KL} [p_m(D_t|\theta_{t,m}) || p_0(D_t)] \approx \frac{1}{L} \sum_{l=1}^L \text{KL} [p_m(D_t|\theta_{t,m}^{(l)}) || p_0(D_t)],$$

where $\theta_{t,m} \sim \mathcal{N}(\phi_m, \tau_m \mathbb{I})$. Note that the KLD term itself is a sum over the KLD terms for each (\mathbf{x}, \mathbf{y}) in the support set. In turn, each of these terms is a KLD between categorical likelihoods, which is easily computed. As detailed in the main text, we divide the sum by the number of points in the set to ease the reasoning about the parameters of π_{KL} . We can further achieve an unbiased estimator to the term inside π_{KL} using stochastic mini-batches of tasks, as is standard in the few-shot classification literature.

Finally, assuming a factorization of the τ_m 's, we can simply evaluate the log-density for each prior, and compute their sum. In practice, we use single-sample estimators of the KL term, and compute the prior terms over batches of tasks to reduce the number of forward passes through the network required to compute the objective. The procedure for evaluating the PredCP prior for a batch of B tasks is detailed in Algorithm 2. Here we use the notation $\text{CNN}(\mathbf{x}; \cdot)$ to denote a forward pass through a convolutional neural network using a set of parameters, applied to an input. We treat the output of such a call as the logits of a categorical distribution.

E Logistic Regression Experimental Details

For the logistic regression experiment in Section 6 (Table 1), we used the probabilistic programming language Stan [8] for the implementation of both Markov chain Monte Carlo (MCMC) and variational inference (VI) [31]. In both cases, we performed inference for the full posterior $p(\beta, \lambda, \tau | \mathbf{X}, \mathbf{y})$. Following Pironen and Vehtari [44]'s implementation, we used a non-centered parameterization: $\beta_d = \lambda_d \cdot \tau \cdot \xi_d$, $\xi_d \sim \mathcal{N}(0, 1)$. For MCMC, we left Stan at its default settings. We evaluated the

Algorithm 2 Single sample evaluation of π_τ for modular meta-learning

Input: Global parameters $\{\phi_m\}_{m=1}^M$, network architecture CNN
Input: Prior π_{KL} , current values $\{\tau_m\}_{m=1}^M$
Input: Inputs from all tasks in batch $\{\{\mathbf{x}_{n,b}\}_{n=1}^N : b = 1, \dots, B\}$

Compute $p_0^{n,b} \leftarrow \text{CNN}(\mathbf{x}_{n,b}; \phi)$
For $m = [1, M]$:
 Sample $\theta_m \sim \text{N}(\phi_m, \tau_m \mathbb{I})$
 Compute $p_m^{n,b} \leftarrow \text{CNN}(\mathbf{x}_{n,b}; \phi, \theta_m)$
 Compute $\text{KL}_m \leftarrow \frac{1}{NB} \sum_{n,b} \text{KLD}(p_m^{n,b}, p_0^{n,b})$
 Compute $\log \pi_m \leftarrow \log \pi_{\text{KL}}(\text{KL}_m) + \log \left| \frac{\partial \text{KL}_m}{\partial \tau_m} \right|$
Return $\sum_{m=1}^M \log \pi_m$

predictive log-likelihood using 4000 posterior samples (the default output). For VI, Stan uses a mean-field Normal posterior, appropriately transforming all variables so that their support is \mathbb{R} . Again we left all hyper-parameters at their defaults. The predictive log-likelihood was evaluated with 1000 samples drawn from the approximate posterior. For the PredCP, we used 10 samples to evaluate the Monte Carlo expectation over $\theta|\tau$ for colon and breast. For allaml, we used only one Monte Carlo sample due to the data set being larger and requiring more time to run the MCMC. The allaml and colon data sets were downloaded from <http://featureselection.asu.edu/datasets.php>. breast was downloaded from <https://archive.ics.uci.edu/ml/datasets/Breast+Cancer+Coimbra>. We standardized the features using the z-transform $(x - \hat{\mu})/\hat{\sigma}$, which we found to improve the speed at which the MCMC converged. We made 20 80% - 20% train-test splits for all three data sets. We left out 10% of the training set for each as a validation set that we ultimately did not use.

F Resnet Regression Experimental Details

For the resnet regression experiment in Section 6 (Table 2), we followed the experimental framework of Nalisnick et al. [37]¹ (which followed Gal and Ghahramani [18] and Hernández-Lobato and Adams [25]). All networks had two hidden layers, ReLU activations, and no batch or layer normalization. The posterior was approximated as:

$$p(\{\mathbf{W}_l, \lambda_l, \tau_l\}_{l=1}^3 | \mathbf{y}, \mathbf{X}) \approx \prod_{l=1}^3 q(\mathbf{W}_l) q(\lambda_l) q(\tau_l) = \prod_{l=1}^3 \text{N}(\mathbf{W}_l; \mu_l, \text{diag}\{\Sigma_l\}) \delta[\lambda_l] \delta[\tau_l]. \quad (20)$$

The weight approximation (Bayes-by-backprop [6], fully factorized Gaussian) was optimized using Adam [28] with a learning rate of 1×10^{-3} (other parameters left at Tensorflow defaults), using mini-batches of size 32, and run for 4500 epochs. The Monte Carlo expectations in the ELBO and PredCP both used 10 samples and *flipout* [54] for decorrelation. The ARD scales λ could be updated in closed-form for all models. The PredCP does not allow for a closed-form τ update (for ADD) and so we used an iterative maximization step. We used only one step per update so that the PredCP’s training time was comparable to the other models’. The UCI data sets were standardized and divided into 20 90% - 10% train-test splits, following Hernández-Lobato and Adams [25]. The test set RMSE was calculated using 500 samples from the $\text{N}(\mathbf{W}_l)$ posterior. For the fixed scale model, we selected the better performing of $\tau_0 = \{.1, 1\}$. For the PredCP, we used the log-Cauchy(0, 1) KLD prior, finding it worked well in the logistic regression experiment and generated sensible sample functions. In Algorithm 3, we provide pseudo-code for evaluating the depth-wise (log) PredCP.

G Few-Shot Classification: Experimental Details and Additional Results

We provide experimental details and results for our few-shot classification experiments.

¹https://github.com/enalisnick/dropout_icml2019

Algorithm 3 Evaluating the Depth-Wise Log-PredCP

Input: Scales τ_1, \dots, τ_L , prior $\pi_{\text{KL}}(\kappa)$, number of Monte Carlo samples S , feature matrix \mathbf{X}
Initialize $\pi \leftarrow 0$
Initialize $p_0 \leftarrow p(\mathbf{y}|\mathbf{X}, \mathbf{W}_{\text{in}}, \mathbf{W}_{\text{out}})$
For $l = [1, L]$:
 Sample $\hat{\mathbf{W}}_{l,1}, \dots, \hat{\mathbf{W}}_{l,S} \sim p(\mathbf{W}_l|\tau_l)$
 For $s = [1, S]$:
 Compute $p_{+,s} = p(\mathbf{y}|\mathbf{X}, \mathbf{W}_{\text{in}}, \{\hat{\mathbf{W}}_{j,s}\}_{j=1}^l, \mathbf{W}_{\text{out}})$
 Compute $\hat{\kappa}_l = \frac{1}{S} \sum_{s=1}^S \text{KL}[p_{+,s}||p_{0,s}]$
 Update $\pi \leftarrow \pi + \log \pi_{\text{KL}}(\hat{\kappa}_l) + \log |\partial \hat{\kappa}_l / \partial \tau_l|$
 Update $\{p_{0,1}, \dots, p_{0,S}\} \leftarrow \{p_{+,1}, \dots, p_{+,S}\}$
Return π (*log-PredCP*)

G.1 Data Details

We use two standard few-shot classification benchmarks for our experiments: mini-ImageNet [53] and few-shot CIFAR100 (FC; [39]). For mini-ImageNet, images are first down-sampled to 84x84, and then normalized. For FC, the images are classified in their 32x32 format after normalization. We use the standard split as suggested by Vinyals et al. [53] for mini-ImageNet, containing 64 training classes, 16 validation classes, and 20 test classes. For FC, we follow the protocol proposed by Oreshkin et al. [39], using the CIFAR100 super-classes to split the data. See Oreshkin et al. [39] supplementary for full details. An $N - \text{way}, K - \text{shot}$ task is randomly sampled according to the following procedure:

- Sample N classes from the appropriate set uniformly at random.
- For each class, sample K examples uniformly at random for the context / support set.
- For each class, sample 15 examples uniformly at random for the target / query set.

Evaluation is conducted by randomly sampling 600 tasks from the test set. Average accuracy and standard errors are reported.

G.2 Network Architectures

For all tasks, we use the standard convolutional architecture proposed by Finn et al. [14]. Each network is comprised of four convolutional blocks, followed by a linear classifier. For mini-ImageNet, we use a standard 3x3 convolution with 32 channels, followed by a max-pool (stride 2), a ReLU non-linearity, and a batch normalization layer. We flatten the output of the final layer, leading to an 800d representation, which is then passed through the linear classifier.

For FC, we employ the same architecture, but with 64 channels, and no max-pooling. A global-average pooling is applied to the output of the final convolutional layer, resulting in a 64d representation, which is then passed through the linear classifier.

We used the standard hyper-parameters proposed by Finn et al. [14], without any tuning. In particular, we use 5 gradient steps for the inner loop during training, and 10 at test time. The inner learning rate is fixed to 0.01, and the meta-learning rate is 1e-3. We use a meta-batch size of 4, and train all models for 60,000 iterations.

G.3 Hyper-Priors and Additional Results

For the modular shrinkage model, we experiment with four hyper-priors: Half-Cauchy, log-Cauchy, a mixture of Gamma and Exponential (GEM), and standard Exponential. Each of these is experimented with as a standard shrinkage prior, as well as the base prior for the PredCP. The parameters of the hyper-priors are fixed throughout experimentation, and are given as follows:

- Half-Cauchy: $p(\sigma), \pi_{\text{KL}} = \text{half-Cauchy}(1.0)$
- Log-Cauchy: $p(\sigma), \pi_{\text{KL}} = \text{log-Cauchy}(2.0)$
- GEM: $p(\sigma), \pi_{\text{KL}} = 0.5 (\Gamma(0.2, 2.0) + \text{Exp}(0.5))$
- Exponential: $p(\sigma), \pi_{\text{KL}} = \text{Exp}(0.5)$

Table 4: Complete results for few-shot classification with few-shot CIFAR100. Considering four priors for σ MAML and four base priors for PredCP.

Beta	Half-Cauchy		Log-Cauchy		Gem		Exponential	
	1-shot	5-shot	1-shot	5-shot	1-shot	5-shot	1-shot	5-shot
PREDCP								
1e-0	33.2 \pm 1.8	51.7 \pm 0.9	37.7 \pm 1.7	51.8 \pm 0.9	37.9 \pm 1.9	52.0 \pm 0.97	38.9 \pm 1.8	51.4 \pm 1.0
1e-1	39.6 \pm 1.6	51.4 \pm 0.9	37.9 \pm 1.9	50.6 \pm 0.7	40.9 \pm 1.8	51.7 \pm 0.9	39.5 \pm 1.9	51.1 \pm 0.8
1e-2	38.2 \pm 1.8	50.9 \pm 0.8	40.1 \pm 1.9	52.5 \pm 0.9	37.8 \pm 1.8	51.6 \pm 0.8	40.3 \pm 1.9	49.1 \pm 1.1
1e-3	39.7 \pm 1.9	52.9 \pm 0.9	40.2 \pm 1.8	50.6 \pm 1.0	38.8 \pm 1.8	51.3 \pm 0.9	38.5 \pm 1.8	50.8 \pm 0.9
1e-4	37.4 \pm 1.7	52.7 \pm 0.9	37.7 \pm 1.8	50.5 \pm 0.9	35.8 \pm 1.7	51.5 \pm 0.9	41.2 \pm 1.8	50.9 \pm 0.9
SHRINKAGE PRIORS								
1e-0	36.9 \pm 1.8	51.4 \pm 0.9	39.5 \pm 1.9	52.2 \pm 1.1	39.8 \pm 1.8	52.4 \pm 0.9	39.4 \pm 1.8	52.6 \pm 0.7
1e-1	39.8 \pm 1.9	52.7 \pm 0.8	40.9 \pm 1.9	52.7 \pm 0.9	36.6 \pm 1.8	52.5 \pm 0.8	38.7 \pm 1.9	51.6 \pm 1.1
1e-2	38.2 \pm 1.8	52.0 \pm 0.9	38.8 \pm 1.7	51.2 \pm 0.8	36.4 \pm 1.8	51.4 \pm 0.9	39.1 \pm 1.9	52.2 \pm 0.9
1e-3	39.3 \pm 1.7	51.3 \pm 0.7	35.9 \pm 1.8	50.8 \pm 0.9	40.8 \pm 1.9	51.9 \pm 1.0	37.5 \pm 1.9	52.2 \pm 0.8
1e-4	38.6 \pm 1.7	51.5 \pm 0.9	40.9 \pm 1.8	50.1 \pm 0.9	38.8 \pm 1.8	51.8 \pm 0.9	40.1 \pm 1.8	51.4 \pm 0.9
MAML (flat θ_t prior)	35.6 \pm 1.8	50.3 \pm 0.9						
σ MAML (flat τ prior)	39.3 \pm 1.8	51.0 \pm 1.0						

Table 5: Complete results for few-shot classification with mini-ImageNet. Considering four priors for σ MAML and four base priors for PredCP.

Beta	Half-Cauchy		log-Cauchy		GEM		Exponential	
	1-shot	5-shot	1-shot	5-shot	1-shot	5-shot	1-shot	5-shot
PREDCP								
1e-0	33.4 \pm 1.7	60.7 \pm 0.8	28.6 \pm 1.6	59.8 \pm 0.8	28.7 \pm 1.6	59.1 \pm 0.8	30.2 \pm 1.7	59.1 \pm 0.8
1e-1	47.9 \pm 1.7	60.4 \pm 0.9	49.3 \pm 1.7	60.4 \pm 0.7	47.5 \pm 1.9	61.4 \pm 0.8	47.7 \pm 1.7	60.6 \pm 0.9
1e-2	47.0 \pm 1.8	60.3 \pm 0.7	45.9 \pm 1.6	60.7 \pm 0.8	46.7 \pm 1.8	61.7 \pm 0.7	47.2 \pm 1.9	61.9 \pm 0.9
1e-3	46.4 \pm 1.7	61.3 \pm 0.8	48.1 \pm 1.8	61.2 \pm 0.9	47.9 \pm 1.7	60.5 \pm 0.8	46.9 \pm 1.7	60.5 \pm 0.8
1e-4	47.7 \pm 1.8	60.4 \pm 0.9	47.7 \pm 1.8	60.3 \pm 0.9	48.1 \pm 1.9	60.1 \pm 0.9	48.3 \pm 1.8	60.4 \pm 0.9
SHRINKAGE PRIORS								
1e-0	42.9 \pm 1.8	57.3 \pm 0.9	48.5 \pm 1.7	60.9 \pm 0.9	24.7 \pm 1.5	29.0 \pm 0.7	44.5 \pm 1.8	57.8 \pm 0.9
1e-1	46.5 \pm 1.8	59.2 \pm 0.9	47.2 \pm 1.8	59.7 \pm 0.9	45.8 \pm 1.8	58.7 \pm 0.8	47.0 \pm 1.8	59.6 \pm 0.9
1e-2	46.8 \pm 1.7	59.3 \pm 0.8	46.3 \pm 1.9	59.3 \pm 0.8	46.7 \pm 1.7	60.1 \pm 0.7	46.8 \pm 1.8	59.1 \pm 0.9
1e-3	47.3 \pm 1.9	59.2 \pm 0.9	47.7 \pm 1.7	59.3 \pm 0.9	47.2 \pm 1.9	60.1 \pm 0.9	47.5 \pm 1.9	59.5 \pm 1.0
1e-4	46.7 \pm 1.8	59.2 \pm 0.9	47.4 \pm 1.7	60.2 \pm 0.7	48.0 \pm 1.5	59.5 \pm 0.9	47.8 \pm 1.7	58.6 \pm 0.9
MAML (flat θ_t prior)	45.6 \pm 1.8	58.4 \pm 0.9						
σ MAML (flat τ prior)	47.4 \pm 1.8	60.1 \pm 0.9						

Additionally, we experimented with a vague (flat) prior, which recovers the model proposed by Chen et al. [11]. In addition, we also add a constant weight β , which multiplies the prior on σ in the outer-loop objective for both the regular shrinkage and PredCP. For each prior, we experiment with $\beta \in \{1e-0, 1e-1, 1e-2, 1e-3, 1e-4\}$.

Tables 4 and 5 provide our complete results for these experiments. For both datasets, and for both 1- and 5-shot, we observe that a PredCP prior with appropriate weighting on the prior term provides the best performance in terms of accuracy on the test set.